May 1988 LRP 347/88

Papers contributed to the
15th EUROPEAN CONFERENCE ON CONTROLLED
FUSION AND PLASMA HEATING

Dubrovnik (Cavtat), Yugoslavia, May 1988

ALFVEN WAVE COUPLING IN LARGE TOKAMAKS

G.G. Borg, A.J. Knight, J.B. Lister, K.Appert and J.Vaclavik

Centre de Recherches en Physique des Plasmas
Association Euratom - Confédération Suisse
E.P.F.L., Lausanne, Switzerland

Supplementary plasma heating by Alfvén waves (AWH) has been extensively studied both theoretically and experimentally for small, low temperature plasmas. However, only a few studies of AWH have been performed for fusion plasmas. In this paper the cylindrical kinetic code ISMENE [1] is used to address problems of AWH in a large tokamak. The results of calculations are presented which show that the antenna loading scales with frequency and vessel dimensions according to ideal MHD theory. A sample scaling of the experimental antenna loading measured in TCA to the loading predicted for a fusion plasma is presented. We discuss whether this loading leads to a realistic antenna design. The choice of a suitable antenna configuration, mode number and operating frequency is presented for NET parameters with a typical operating scenario.

Introduction : In a hot plasma, AWH is effected by antenna excitation of a fast magnetosonic wave which mode converts to the kinetic Alfvén wave (KAW) at surfaces in the plasma where the Alfvén wave dispersion relation is satisfied locally [2]

$$\omega^2(\varepsilon) = [n+m/q(\varepsilon)]^2 \; B_o{}^2/(\mu_o \rho(\varepsilon))/R^2 \qquad (1)$$

In equation (1) n and m are the toroidal and poloidal mode numbers, B_o the total field, R the major radius, ω the operating circular frequency (much less than the ion cyclotron frequency), ρ and q are the plasma mass density and safety factor as a function of ε=r/a, a being the minor radius.

In this study the machine parameters of the NET DN configuration [3] are modified to the cylindrical equivalent values; major radius (R)=5.18 m, minor radius (a)=2.17m, toroidal field (B_o)=5.0T, plasma current (I_p)=10.8MA, burn temperature (T)=14keV (on axis) and electron density (n_e)=$18\times10^{19}m^{-3}$ (on axis) with a 50:50 D/T fuel mixture.

Scaling of Antenna Loading in AWH : Scaling laws allow one to predict the antenna loading at a fixed point in the spectrum (n, m, ε and both antenna and vessel geometry fixed in equation (1)) under a change in ω, R, ρ or B_o.

Scaling laws are useful because:

a) Codes are restricted to simplified plasma, antenna and vessel geometries.
b) Such laws give increased confidence in the loading predictions if the validity of the plasma model has already been established experimentally [2].

According to ideal MHD, the antenna loading at a fixed point in the Alfvén spectrum increases linearly with the driving frequency and is independent of the plasma density and magnetic field.

The antenna loading, R_A, normalised to ω, is plotted versus the logarithm of the on axis density in Fig. 1a using ISMENE for the basic NET dimensions. We have chosen $\varepsilon=0.67$ and $(n,m)=(-1,-1)$, $(-2,-1)$, $(-4,-1)$ and $(-8,-1)$. Satisfactory agreement is obtained for $n=-1$, -2, and -4 for $n_e(0)>10^{18}m^{-3}$. At low densities a discrepancy results from finite frequency effects.

In ideal MHD, the antenna loading scales linearly with the major radius at a fixed point in the spectrum provided that the plasma, antenna and vessel geometries are held fixed. This law is checked by shrinking and expanding the basic NET configuration with ω, B_o constant, $n_e \sim 1/R^2$, $a \sim R$ and $I_p \sim R_p$ so that equation (1) remains invariant. This scaling law is checked in Fig. 1b for $|n|=1$, 2, 4, 8 and $|m|=1$ and demonstrates that an antenna loading obtained in, for example, ASDEX would lead to only a $\sim\pm10\%$ error in predicting the NET loading.

An example of how scaling laws can be used to predict the loading is shown in Fig. 1c. The TCA experimental loading for $n=2$ excitation [2], $f=2.5$ MHz, $R=0.61$ and $B_o=1.51$T is scaled to a NET equivalent loading with $f=0.5$MHz, $R=5.18$ and $B_o=5.0$T. The ISMENE load is adjusted to agree as well as possible with the TCA experiment and the NET equivalent, and scaled loadings are then calculated directly. The agreement is better than 10% in the (2,1) continuum for more than a factor of 8 increase in the vessel dimensions. For $n>2$ the agreement would be somewhat worse due to finite frequency effects.

Choice of Suitable Mode and Frequency : In NET there are 16 oblique and 8 radial access ports equispaced toroidally in each case with a 20cm blanket into which the antenna has to be recessed [4]. In addition, we restrict our discussion to unshielded [2], poloidal antennas although future experiments may reveal the utility of Faraday shields and tilted antennas [5].

In AWH it is desirable to have the largest possible number of antennas due to the phase coherence of the wave launching. Consistent with this, the number and the size of the available ports, we choose 8 low field side poloidal antennas with poloidal half angle 90° and toroidal half angle <5° (Fig. 2a).

Taking into account the Fourier spectrum of the antenna, ISMENE

calculated loads are presented in Fig. 2b for $|n|=1,2,4,8,16$ and $|m|=0,1,3$ using the optimum phasing for each mode, and $\varepsilon=0.67$. This calculation shows that n=4, 8, m=1 and n=16, m=0 at f=1.08, 1.98 and 3.77MHz respectively give the greatest total antenna loading. The maximum load occurs at n=2.5R/a ~6 in agreement with [6] and [7]. This loading at 500-1000mΩ gives an r.m.s. antenna current of 10kA for 50MW power input, and leads to a feasible technological requirement.

It should be noted that the actual loading will depend on the antenna geometry model, in particular the recess. Studies of this question have shown that an antenna flush with the torus wall can have a substantial loading, of the order of 15% of the no-wall case. The flush-wall configuration for a plasma-wall spacing of 0.1m and an equal recess depth, has the same antenna loading for n=8, as an antenna one third away from the same wall without a recess.

The radial location of the principle resonance layers excited during an n=8 and n=4 heating scenario is shown in Fig. 2c during the heating and fuelling phase to ignition in NET [8]. N=8 with all antenna currents in phase at f=2.16MHz begins the heating phase at $\rho=3.6\times10^{-7}kg/m^{-3}$ (D/T) with a change of frequency to 1.08MHz and n=4 at $\rho=4.8\times10^{-7}kg/m^{-3}$. The power deposition is approximately local (20% of the minor radius) and is equally divided between the m/n>0 and the m/n<0 layers.

Conclusion : Calculations have been presented which demonstrate that the scaling laws of ideal MHD can be used to predict antenna loadings in large tokamaks from those obtained in small tokamaks. An $|n|=4$, 8, $|m|=1$ scenario has been discussed.

Acknowledgements : This work was funded under the NET contract 251/86-10/FU CH/NET. We are endebted to Dr. J-G. Wegrowe for stimulating discussions.

References

[1] K. Appert et al. (1987), in Proc. 7th Int. Conf. on Plasma Physics, Kiev, Invited Papers, Vol. 2, 1230.
[2] G. Collins et al., Phys. of Fluids 29 (1986) 2260.
[3] F. Engelmann, 1986, Concept and Parameters of NET, NET Report EUR-fu/XII-80/86/64.
[4] E. Salpietro et al, NET Basic Machine, NET Report, 1988.
[5] F. Hofmann et al., Nucl. Fusion 24 (1984) 1679.
[6] K. Appert et al., (1980) Plas. Phys. and Contr. Fus. Res., Vol. II, IAEA-CN-38/D-1-1.
[7] A.G. Kirov et al., RF Systems for Alfvén Wave Heating of Large Tokamaks, IAEA Technical Workshop on RF Heating and Current Drive, Moscow, 1987.
[8] F. Engelmann et al., NET Physics Basis, NET Report, 1988.

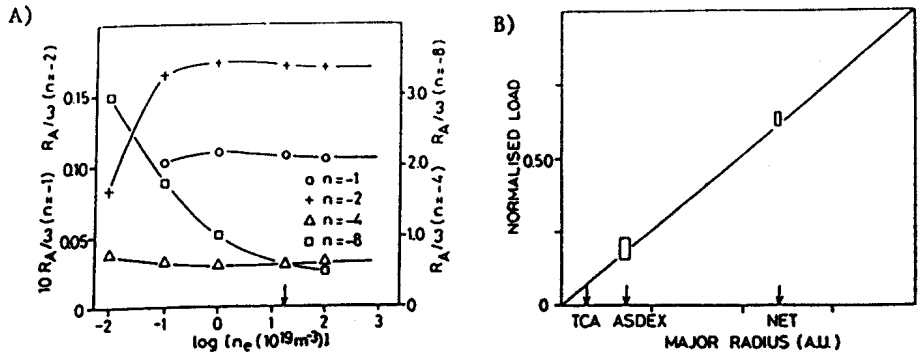

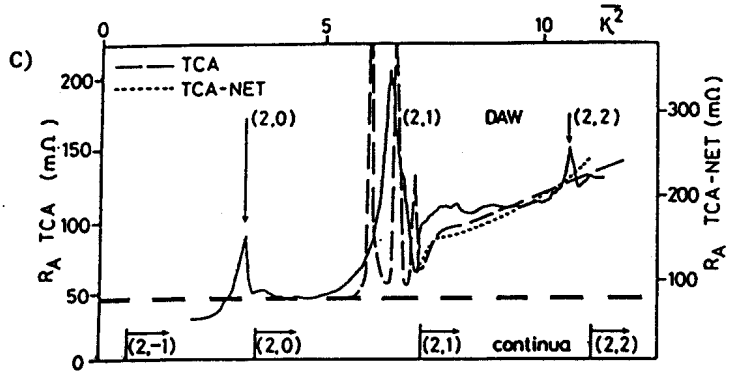

Fig. 1a Scaling of antenna load with frequency.

Fig. 1b Scaling vs major radius

Fig. 1c Scaling of TCA to NET equivalent plasma. Scaled load on right axis.

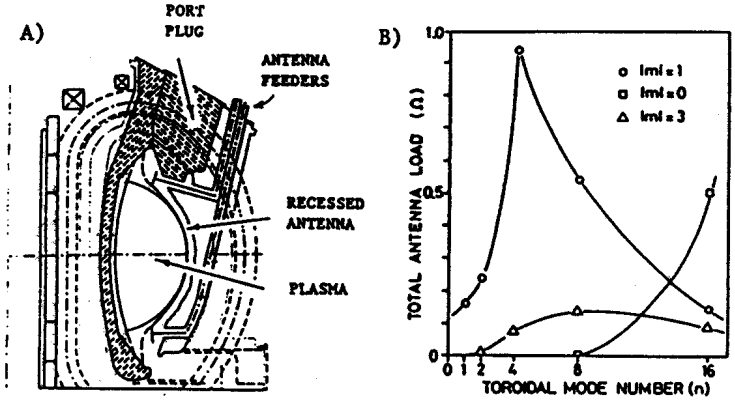

Fig. 2a Antenna configuration in NET.

Fig. 2b Load vs n for 8 sector antenna

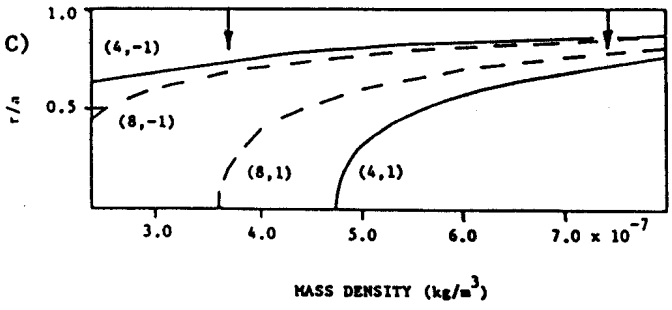

Fig. 2c ARL positions in an n = 4 and 8 heating scenario. Arrows indicate the heating phase.

KINETIC AND CURRENT PROFILE EFFECTS OF ALFVEN WAVES IN THE TCA TOKAMAK

G.G. Borg, A.A. Howling, B. Joye, J.B. Lister, F. Ryter* and H. Weisen

Centre de Recherches en Physique des Plasmas
Association Euratom - Confédération Suisse
E.P.F.L., Lausanne, Switzerland

*present address: IPP, Garching, F.R.G.

Recent Alfvén wave experiments in the TCA tokamak show new evidence of the importance of kinetic effects and the influence of plasma conditions on the Alfvén wave. The R.F. magnetic field measured at the plasma edge reflects unambiguously the resonance of the kinetic wave eigenmodes in the plasma centre. The measured values of the resonance Q-factor of the principal eigenmodes are lower than predicted by the code by a factor of 3 to 20, although all expected damping mechanisms are included in the code. Alternative damping mechanisms are discussed and the best candidates proposed after quantitative evaluation. The R.F. itself modifies the plasma in such a way that the coupling strength can change very strongly. The experimental observations and the results of the code show that the current profile is certainly the best candidate which can affect the coupling in this way, implying that the R.F. pulse is able to influence the plasma current profile.

Observations of kinetic effects at the edge : In the kinetic description of AWH, the surface compressional wave mode converts to the KAW in the vicinity of the Alfvén Wave resonance layer (ARL). As the ARL moves outwards, standing waves of increasing order are formed due to reflection at the plasma centre. These standing waves, which occur for all (n,m) modes, appear as a sequence of resonances on the loading and edge plasma wavefield at a higher density than the principle DAW.

A comparison between experiment and the cylindrical kinetic code ISMENE [1] for the n=2 edge plasma wavefield is shown in Fig. 1, where the experimental, cold and kinetic theory fields have been plotted in the complex plane. From the figure it may be concluded that the resonances are a kinetic effect. The resonances disappear when the KAW is damped before reaching the plasma centre and so indicate approximately when energy deposition ceases to be central.

Width of the DAW resonance peaks : An important discrepancy between theory and experiment is the value of the quality factor, Q, for the DAW resonances. Figure 2a shows the experimental (2,1) Q as a function of

plasma current and R.F. power and Fig. 2b shows the theoretical Q for two representative current profiles as a function of plasma current. According to Fig. 2a, the DAW affects the plasma in such a way that its Q increases with R.F. power.

A comparison of the figures shows that the experimental Q is about 10 times lower than the theoretical Q, even though the kinetic code includes those damping mechanisms, electron Landau damping, transit time magnetic pumping and electron-ion collisions, known to be important for the damping of shear Alfvén waves. The theoretical Q is not a strong function of the electron temperature, or its profile.

Three mechanisms have been proposed which could lead to a lower Q than predicted and which are not contained in the model of a hot quiescent plasma.

Enhanced collision frequency due to MHD turbulence has been observed to lead to lower than predicted Q's for magnetoacoustic waves [2]. Calculations using the kinetic code with 1000 times the electron-ion collisionality revealed a negligible change in Q since the kinetic damping mechanisms dominate for TCA conditions. Turbulence enhanced electron-ion collisions do not therefore explain the low observed Q.

In toroidal geometry a DAW may couple to KAWs of several different surfaces already present in the plasma. This coupling, not contained in the cylindrical theory, could provide an additional energy loss channel for the DAW. Analysis of such coupling would require a 2D kinetic code. However, we have made numerical simulations based on coupled circuits, using the experimental observation that the KAW $\tilde{n}_e$ at the (2,0) resonant layer increases by a factor of 5 during the passage of the (2,1) DAW. These reveal that the power transfer is insufficient to explain the observed Q. Until toroidal coupling is properly modelled, however, the energy loss of the DAW cannot be determined unambiguously.

Since the DAW resonance is density and plasma current dependent, a noise modulation of the average values of these parameters, or their profiles, will modulate the resonance condition and lead to a smearing of the resonance curve. Changes of ~ 3 % in $\bar{n}_e$ and ~ 10 % in $I_{p,}$ required to reduce Q enough, would be too large. Plasma current and density profile wobulations are, therefore, most likely responsible for the low observed Q.

Effect of R.F. power on the Alfvén Wave spectrum : At high power levels in AWH, discontinuities are observed to occur in the plasma parameters at the continuum thresholds [3]. At the thresholds, the rate of density rise decreases or even changes sign and a drop in the plasma internal inductance (l_i) has been proposed to accompany a transient drop in R_{pl} [3,4].

Further evidence for a drop in l_i is shown in Fig. 3a. The density begins to decrease after the (2,1) threshold, however, the DAW fails to

reappear due to a drastic loss of loading as the spectrum is reswept. This is surprising since the DAW is relatively insensitive to plasma parameters provided the profiles of density and current are held fixed. The DAW loading decreases very rapidly for flat density profiles as the profiles become flatter; however, the change in density profile required to completely eliminate the DAW is larger than measured. Numerical calculations show that the DAW loading and coupling (R_{ant}/Q) are also strong functions of the plasma current profile, increasing linearly with l_i as shown for the coupling in Fig. 3b for the (2,1) DAW over a wide range of current profiles. Fig. 3b indicates that a flattening of the current profile can cause the DAW coupling to become vanishingly small, however, the interpretation is complicated by the presence of β in the experimental $\Lambda = (\beta + l_i/2)$ measurement. The problem of current profile modification is also treated in [5].

Conclusion : Results have been presented which show clear evidence that certain effects of Alfvén waves cannot be explained by the simple quiescent cold plasma MHD theory. Kinetic effects must be included to fully describe the standing KAWs observable in the edge plasma wavefield. Current or density profile wobulation appears the best candidate to explain the low observed Q. Static current profile changes occurring at continuum thresholds seem the best candidate to explain a markedly reduced DAW loading in experiments where the spectrum is reswept by a descending density.

Acknowledgements : This work was partly funded by the Fonds National Suisse de la Recherche Scientifique.

References

[1] Appert et al., (1987), in Proc. 7th Int. Conf. on Plasma Physics, Kiev, Invited papers Vol. 2, 1230.
[2] C. Ritz et al., (1982), Hel. Phys. Acta 55, p. 354.
[3] G. Besson et al., (1986), Plas. Phys. and Contr. Fuscon. 28, p. 1291
[4] K. Appert et al., (1987), in Proc. 7th Int. Conf. on Plasma Physics, Kiev
[5] Th. Dudok de Wit et al., (1988), Alfvén Wave Heating and its effects on the Tokamak Current Profile, this conference.

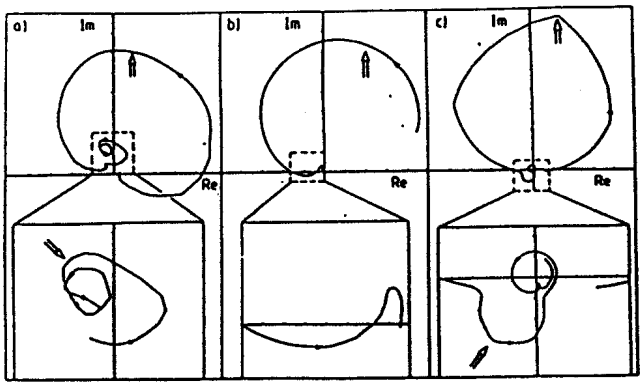

FIG. 1. The RF magnetic wavefield of the (2,1) DAW and KAW resonances plotted in the complex plane: a) experiment b) cold model c) kinetic model.

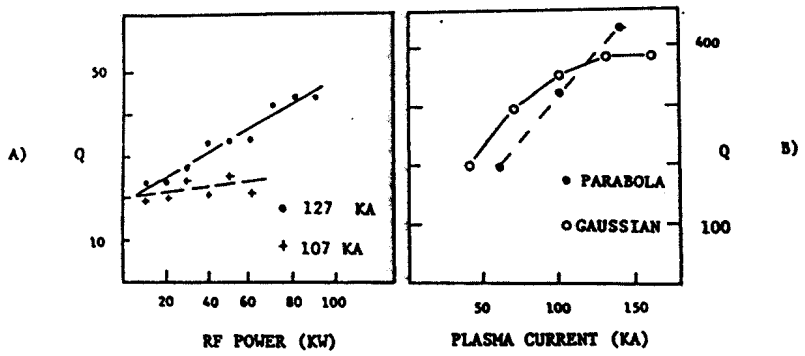

FIG. 2 A) measured Q of(2,1) DAW vs RF power.
B) Calculated Q of (2,1) DAW vs plasma current. using a parabolic and a Gaussian profile.

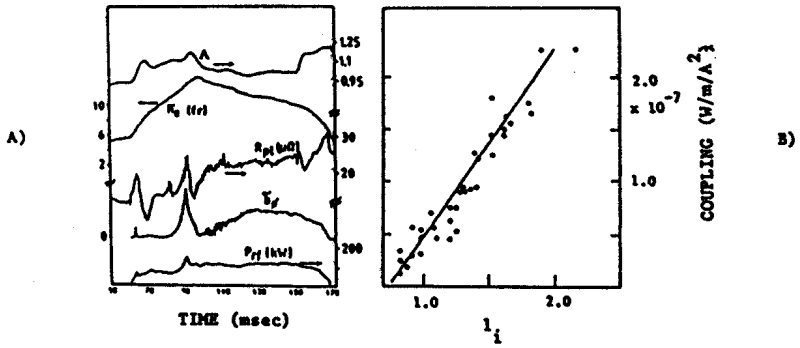

FIG. 3 A) Loss of coupling to DAW during density fall. Note change in lambda.
B) DAW coupling vs plasma internal inductance calculated from code using a wide range of plasma current profiles.

ALFVEN WAVE HEATING AND ITS EFFECT ON THE TOKAMAK CURRENT PROFILE

T. Dudok de Wit, A. A. Howling, B. Joye and J. B. Lister

Centre de Recherches en Physique des Plasmas
Association Euratom - Confédération Suisse
E.P.F.L., LAUSANNE (Switzerland)

The aim of this paper is to interpret the effect of Alfvén Wave Heating (AWH) on the current, density and temperature profiles of the TCA Tokamak plasma. AWH is accompanied by significant increases in line-averaged density $\overline{n_e}$ and $(\beta_p + l_i/2)$ [1], where $(\beta_p + l_i/2)$ is deduced from the equilibrium values of plasma current and vertical field (after correcting for the vertical field penetration L/R time of 1.1 ms for the vacuum vessel). For given plasma conditions, the value of $(\beta_p + l_i/2)$ does not depend sensitively on the exact major radius of the plasma (determined by using different position feedback methods which controlled the magnetic axis or the outermost flux surface). We therefore have confidence in the accuracy of the $(\beta_p + l_i/2)$ measurement.

In the absence of a reliable diamagnetic loop measurement for β_{perp}, the contributions of β_p and l_i must be separately evaluated and it is here that different interpretations may arise. In what follows, we present the observations which support the hypothesis of current profile (l_i) changes and discuss how these conjectured changes might be induced by AWH. We then compare this scenario with one in which increases in plasma energy (β_p) are presumed to account for the increase in $(\beta_p + l_i/2)$, in order to determine whether β_p, l_i, or a combination of both are responsible for these changes.

Current Profile Changes. Strong evidence for the effect of AWH on the current profile comes from the changes in amplitude of the Mirnov activity (associated with a modification of the current density gradient near the q=2 surface) closely linked with the appearance of AW thresholds in the plasma which can, in extreme cases, lead to spectral-related disruptions [2]. Further evidence includes changes in sawtooth frequency [3], and the phenomenon of hysteresis in which the loading of the global resonances (or Discrete Alfvén Wave DAW) is observed to depend on $(\beta_p + l_i/2)$ changes, while a 1-D kinetic code predicts that the DAW loading does depend on l_i [4]. We have considered two schemes in which AWH could be changing the current profile:

Heating at the AW resonance surfaces. Firstly, it was proposed that the dissipation of the Kinetic Alfvén Wave (KAW), excited at its AW resonance surface, may locally heat the plasma hence causing a current profile modification. However, there is no X-ray flux response coincidental with the passage of the resonance surfaces as they move outwards during the AW-induced density rise, and (β_p+ l_i /2) tends to decrease instead of increase when a new resonance layer appears near the centre of the plasma. RF power modulation experiments demonstrate that there is in fact evidence for indirect AWH and that this energy is deposited at the q=1 surface [5]. The model of current profile modification due directly to resonance surface heating is therefore inadequate.

Current Drive by AWH. Secondly, it has been suggested that the KAW drives current by electron Landau damping, the required asymmetry for driving a net current with a symmetric antenna being due to the plasma gyrotropy. Parallel or anti-parallel current drive associated with resonance surfaces near the edge would then strongly influence the ohmic current density profile. This model was tested by separately driving travelling waves with toroidal mode number n=+1 and n=-1. Direct antenna voltage measurements were used to estimate the ratio of AW power in each direction. Using phase shift circuits in the individual AW-generator final stages, a power ratio of better than 1000 was obtained for n=+/- 1 waves. The spectral purity obtained was confirmed by the change in wavefields, the lifting of the degeneracy in the (n,m) = (+1,+1) and (-1,-1) DAWs, and detailed observations of the density fluctuations due to the KAW [6]. The macroscopic parameters of the plasma however were unaltered; the (β_p+ l_i /2) trace differed between the n=+1 and n=-1 cases only briefly after the appearance of the DAW threshold, and even then by less than by 0.04. This result is comparable to the change in l_i obtained with a semi-analytical model which assumes that current is driven at the AW resonance surface by transfer of momentum to non-trapped electrons. This experiment would seem to definitively deny the influence of direct AW current drive, although it might be claimed that higher-n travelling waves (which cannot be produced with the four pairs of antennae on TCA) could possibly drive current.

Changes in the Plasma Energy Content. Since it is difficult to positively measure a current profile change, a simple analysis of (β_p+ l_i /2) was performed on plasmas in different conditions for which the following assumptions were made:

a) the plasma energy remains constant; or

b) the current profile remains unaltered.

The solid lines in Fig.1 represent an AWH discharge, the dashed lines refer to an ohmic discharge and will be explained afterwards. An increase in (β_p+ l_i /2) is always observed at the onset of the RF pulse. The range of values of β_p represented by the shaded area were calculated assuming that the electron and ion temperatures did not change (giving the lower line), and assuming that the ion temperature increased linearly with the AWH-induced density

rise (giving the upper β_p trace). The range of β_p in the figure is therefore due to the density change and the reasonably-expected variation in ion temperature [7] due to increased electron-ion power transfer. The observed transient broadening of the density profile [8] and the peaking of the temperature profiles each have a relatively small effect which tend to cancel, thus leaving the value of β_p unaltered.

Figure 1a) shows the range of values of l_i calculated from the $(\beta_p + l_i/2)$ trace and the calculated β_p trace, ie assuming that no electron heating occurs. Note that an initial peaking in the current profile is predicted.

Figure 1b) shows the range of values of T_e (normalised to the initial ohmic value) necessary to account for the measured $(\beta_p + l_i/2)$ on the assumption that l_i does not change from its ohmic value. A rise and fall of the electron temperature is always predicted.

These two figures thus represent the two possible extremes of current profile change with no electron heating (Fig 1a) and electron heating with constant current density profile (Fig 1b).

The heavy dashed line in Fig 1b is a Thomson scattering measurement of T_e on axis. We note that the trend in T_e is similar, although the observed temperature change is not sufficiently large to explain the $(\beta_p + l_i/2)$ variation in terms of the fixed current profile model. It is clear that only a compromise between the two extreme models can explain the $(\beta_p + l_i/2)$ and T_e measurements, ie simultaneous changes in both the electron temperature and the current profile are necessary to account for the large increase in $(\beta_p + l_i/2)$. If l_i were assumed not to change, an astonishingly high AW heating efficiency would be deduced.

In order to check that temperature and profile changes are not simply due to the AWH-induced density rise, the parameters of an ohmic gas-puffing shot, with a similar initial density rise, are superimposed with dashed lines. Small changes in l_i or T_e, according to the model used, also occur, but clearly the AWH causes significantly larger increases. This general behaviour was consistently reproduced for a wide range of plasma currents.

<u>Conclusions.</u> AWH does not appear to be significantly influencing the current density profile by direct heating associated with resonance surfaces, or by current drive by the Kinetic Alfvén Wave. However, a comparison with gas-puffing shots (which can reproduce the initial rate of density rise) indicates that AWH does lead to electron temperature heating and some current profile peaking at the onset of RF heating, and that both of these must be included before the increase in $(\beta_p + l_i/2)$ can be explained.The mechanism by which these changes occur remains to be explained - it may involve a change in confinement. This mechanism would also have to account for the observed spectral-related phenomena. The installation of full antenna screens, to investigate the possible elimination of the AWH-induced density rise [9], and experiments with prolonged plasma pulses in which steady-state condtions could be achieved, will provide many answers to the questions of heating and profile changes during AWH.

Acknowledgements. We wish to thank the TCA team for its technical support. This work was partially supported by the Fonds National Suisse de la Recherche Scientifique.

References.

[1] JOYE B. et al - paper presented at this conference.
[2] APPERT K. et al - (Invited paper) Intl. Conf. Pl. Phys. Kiev, USSR April (1987)
[3] BESSON G. et al Pl. Phys. and Contr. Fus. 28 1291 (1986)
[4] BORG G. G. et al - paper presented at this conference.
[5] JOYE B. et al 'Dynamical plasma response to additional heating.' Accepted for publication in Pl. Phys. and Contr. Fus. (1988)
[6] BEHN R. et al Pl. Phys. and Contr. Fus. 29 75 (1987)
[7] De CHAMBRIER A. et al - to be submitted to Pl. Phys. and Contr. Fus.
[8] COLLINS G. A. et al 12th Eur. Conf. Contr. Fus. and Pl. Phys. Budapest 2 248 (1985)
[9] BALLICO M. J. et al - submitted to Pl. Phys. and Contr. Nuc. Fus

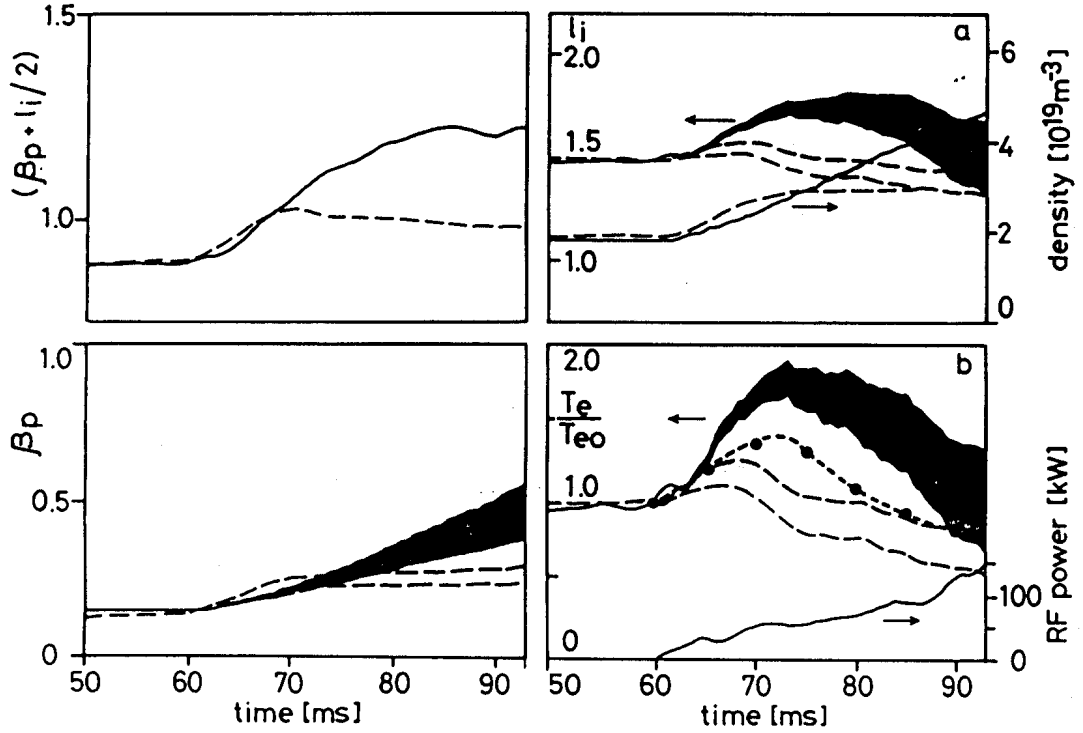

Figure 1 Measured $(\beta_p + l_i/2)$ trace and estimated β_p range allowing for T_i increases, with the consequent variations in:
a) l_i (assuming no change in T_e) and b) T_e (assuming no profile changes).
Solid lines: Alfvén Heated plasma, dashed lines: gas-puffing into an ohmic plasma
- - ● - - $T_e(0)$ from Thomson scattering. Plasma current = 120kA

EFFECTS OF THE ALFVEN WAVE HEATING ON THE TCA PLASMA STUDIED BY THE DYNAMICAL RESPONSE

B. Joye, J.B. Lister and J.-M. Moret

Centre de Recherche en Physique des Plasmas
Association Euratom - Confédération Suisse
EPFL - LAUSANNE (Switzerland)

Studies of the dynamical response of the plasma to modulated Alfvén Wave Heating (AWH) power and to modulated gas puffing in ohmic conditions have been performed on TCA. In both cases, the radial profile of the phase of the electron temperature response exhibits a low value inside the q=1 radius, indicating the presence of a central thermal energy source. Absolute comparison of the gain and the phase in the two cases leads to the conclusion that the electron temperature perturbation during AWH is dominated by the influence of the density variation, with a peaked kinetic energy modulation profile. This at least partly explains the previously reported high performances of the AWH results.

Introduction Dynamical plasma response has been extensively used on TCA as a powerful and systematic approach to interpret AWH experiments [1]. The present study concentrates on the analysis of the soft X-ray flux as an electron temperature measurement. Experiments were carried out both during r.f. heating and in purely ohmic conditions.
TCA plasmas (a=0.18 m, R=0.61 m, B_φ=1.52 T) are heated by Alfvén Waves at 2.0 - 2.5 MHz launched by 8 phase-coherent antennae. Dynamical response measurements are performed either by sinusoidally modulating the r.f. power or the gas valve between 50 and 500 Hz or by superimposing a δ function. In the first case, a given signal y(t') is fitted in a time window of 5 to 50 ms to the form : $y(t') = Re(Y(t)) \cdot \cos(\omega t) + Im(Y(t)) \cdot \sin(\omega t) + \langle y \rangle(t) + d\langle y \rangle/dt\ (t) \cdot (t-t')$. This method has the same properties as a classical Fourier transform but allows a good time resolution even with a non-integer number of cycles and transient conditions with significant drift. In the second case, a transmittance, expressed as a rational function of $z=e^{sT}$ (s is the Laplace variable and T the sampling period), is identified by means of the Stieglitz method [2]. The advantage of the latter technique is that the frequency response can be determined in one shot and without using a specific waveform excitation. Comparison of the two analyses gives excellent agreement.

Dynamical response of the electron temperature to AWH Profiles of the normalised gain and of the phase of the soft X-ray response to a modulated r.f. power exhibit two distinct regions : the inner volume of the discharge displays the lowest gains and phases; outside a well defined radius both the gain and the delay increase. A plasma current scan between 55 kA and 125 kA clearly demonstrated that this separation surface is linked to the sawtooth inversion radius : results for 125 kA and 85 kA are plotted in Fig. 1 (a) and (b). At the highest frequencies used ($\geq$ 200 Hz), the phase profile inside q=1 becomes slightly convex. Therefore the outermost part of the inner volume possesses the lowest phase,

accompanied by a small peak on the amplitude, indicating the presence here of a thermal energy source. The large jump in phase outside this radius is associated with the good thermal insulation of the q=1 region, a property also observed on TFR during pellet injection [3]. Surprisingly, the phase profile is not affected by the positions of the resonance layers near which the wave energy is theoretically predicted to be absorbed.

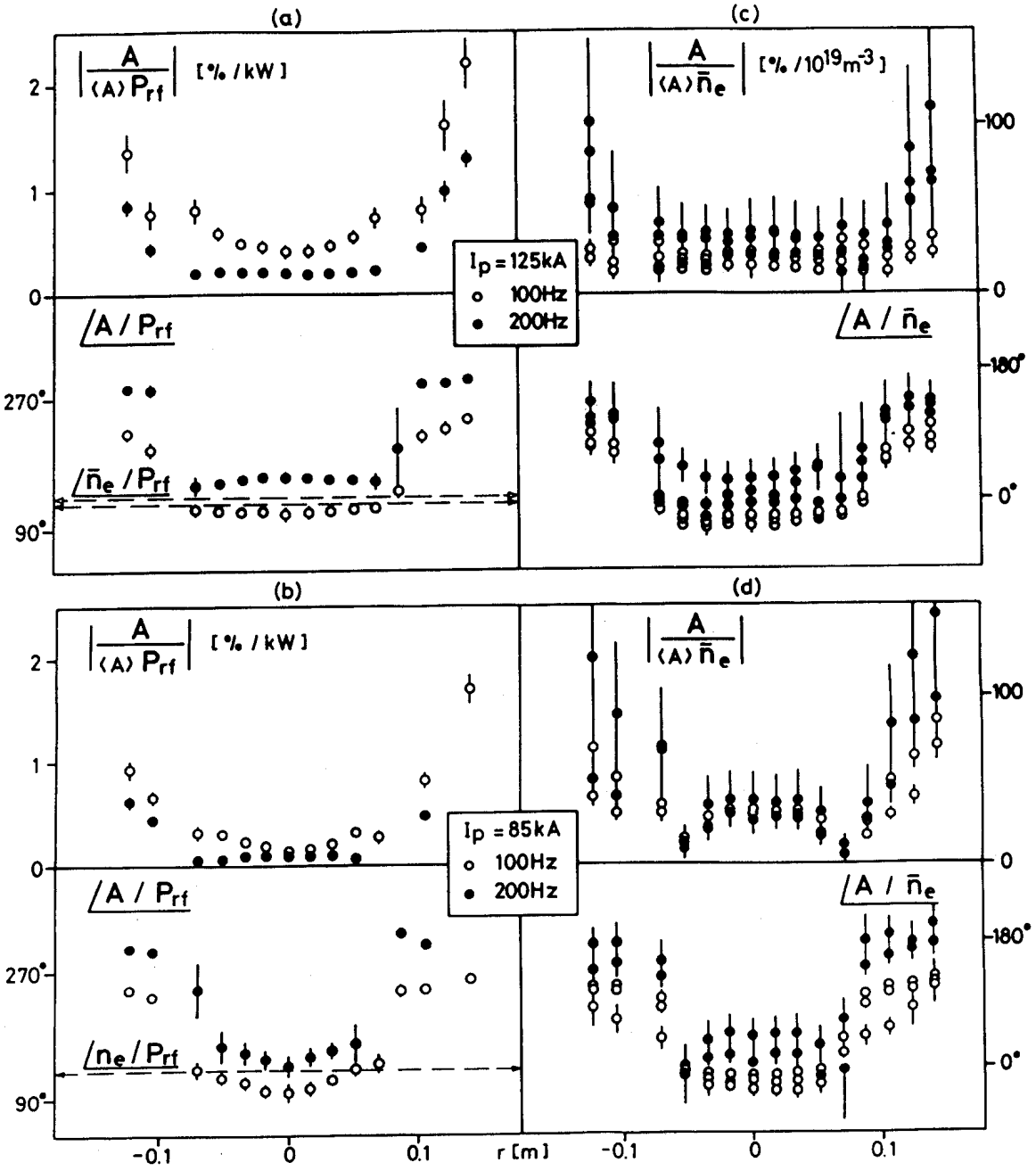

Fig. 1 *Relative gain and phase profile of the response of the soft X-ray, (a) and (b) during r.f. power modulation, (c) and (d) with gas valve modulation, (a) and (c) at 125kA, (b) and (d) at 85kA.*

At modulation frequencies much higher than the inverse local confinement time, the local energy is related to the local power deposition by an integration, giving a phase of 90°. The observed lowest phase however always tends towards 180° at high frequency. The diagnostic spatial resolution (18 mm) was checked to be adequate by carrying out the measurement during a current ramp, in order to make any possible 90° point cross through the visible chords. The only possible explanation in such a case is that the wave energy is not directly thermalised but there is an indirect mechanism driven by the r.f. power subsequently producing a thermal perturbation, such that a 90° delay can be generated. None of the damping mechanisms involved in Alfvén wave absorption has a sufficiently long characteristic time constant to produce this delay.

Dynamical response of the electron temperature to modulated gas puffing

AWH is accompanied by a large density increase. In order to quantify the influence of the density variation , the response of the soft X-ray signals to modulation of the gas valve was measured in purely ohmic discharges (Fig. 1(c, d)). The gain and phase profiles display the same characteristics as before : a low phase inner region and a shrinking of this volume when I_p is decreased. The phase on the axis however is close to zero or even negative, showing that n_e is not the driving mechanism but is only useful for comparison. The parallel can be extended further : if we choose as phase origin the phase between n_e and P_{rf}, the phase profiles cannot be distinguished from each other even in absolute values ; both r.f. power and gas valve modulation produce identical relative amplitudes proportional to $|n_e|$ (Fig. 2). The sawtooth period was previously found to be modulated out of phase by the r.f. power [1], a feature that can also be reproduced by sinusoidal gas puffing.

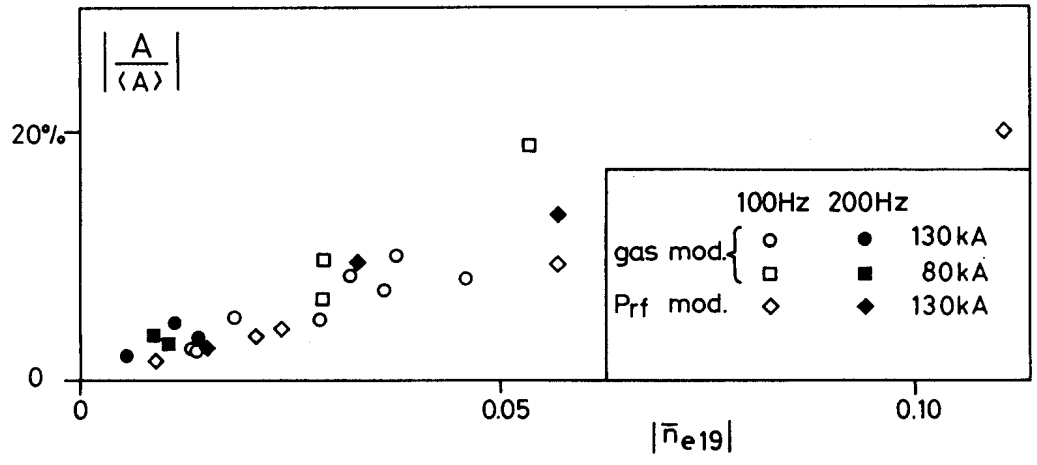

Fig. 2 Relative modulation amplitude during both r.f. power and gas valve modulation as a function of the density modulation amplitude.

Discussion The present discussion addresses the consequences of the previous results to the interpretation of AWH experiments and some considerations about the possible mechanism underlying the observations. A rough estimation of the perturbed electron thermal energy profile gives a peak to mean ration near 5 and in the r.f. case a volume integrated value matching $|P_{rf}|$. This goes a long way to explain previously reported AWH results yielding an astonishingly high heating efficiency and central power deposition estimated by radial power balance [4] or by sawtooth slope analysis [5]. In the case of direct electron heating, the expected modulation amplitude would be comparable to, or smaller than, the observed effect of the density. The superposition of the two contributions would lead, if placed in quadrature, to a maximum phase difference of 45°, experimentally difficult to identify. The dominant role of the density also explains the lack of sensitivity of the phase profile to the resonance layer position. In the two previous cases, a temperature perturbation arising from edge cooling can be discounted, as the source clearly originates inside or near q=1. Modifications of the confinement properties are also excluded : any power dependence of the thermal conductivity would give rise to a phase varying with the r.f. power amplitude, which was not the case in the experiments. The evident link with the current profile via the q=1 radius and the peakedness of the electron kinetic energy modulation amplitude may be symptomatic of a form of temperature profile consistency in both ohmic and heated conditions. A possible modulation of the local ohmic power or a possible exchange between internal poloidal magnetic and plasma kinetic energy cannot be excluded : as experimental evidence, the relative modulation amplitude of the Shafranov parameter $\beta + l_i/2$ is always smaller than the central soft X-ray chord modulation.

Conclusion Dynamical analysis of the plasma response to r.f. power and gas valve modulation have clearly shown that two perturbations can produce similar temperature responses. This response is characterised by a central thermal source certainly linked to the current profile and whose origin remains unknown. This presents an example of the difficulty in interpreting a non-stationary heating experiment while the ohmic behaviour of the target plasma is so badly understood.

Acknowledgement We would like to thank all the members of the TCA team. This work is partially supported by the Fonds National Suisse de la Recherche Scientifique.

References

[1] Joye B. et al., 1988, Dynamical plasma response to additional heating, accepted for publication in Plasma Phys. and Cont. Fus..
[2] de Larminat Ph., Thomas Y., Automatique des systèmes linéaires, Flammarion, Paris.
[3] TFR Group, 1987, 14th EPS Conf. Contr. Fus. Plasma Phys. (Madrid) 1, 29.
[4] A. de Chambrier et al., 1985, X IAEA Conf. on Plasma Phys. and Contr. Nucl. Fus. Research (London) I, 551.
[5] Besson G. et al., 1986, Plasma Phys and Contr. Fus. 28, 1291.

SHAFRANOV PARAMETER LIMITS FOR OHMIC AND R.F. HEATED PLASMAS IN TCA

B. Joye, J.B. Lister and F. Ryter*

Centre de Recherches en Physique des Plasmas
Association Euratom - Confédération Suisse
E.P.F.L, Lausanne, Switzerland

*present address: IPP, Garching, F.R.G.

An ohmic study is presented to define the experimental dependence of the value of $(\beta + l_i/2)$ derived from the Shafranov equation. The Alfvén Wave Heating pulse causes an increase in both $(\beta + l_i/2)$ and density, and with R.F., the value of $(\beta + l_i/2)$ is significantly greater than the ohmic scaling. However, the maximum R.F. values never exceed the maximum achieved ohmic values. As this limit is approached, the m=2 activity increases, as in the ohmic case, and we show that this increase correlates well with the increase in $(\beta + l_i/2)$.

Results : This paper studies the increase in $(\beta + l_i/2)$ measured during Alfvén Wave Heating (f~2.5 MHz) on the TCA tokamak (R, a = 0.61, 0.18 m, $B_\phi \leq 1.51$ T, $I_p < 135$ kA, D_2), and compares the results with ohmically heated discharges. When the R.F. pulse is applied, there is a significant and rapid increase in the value of the Shafranov $(\beta + l_i/2)$ calculated from the vertical field and plasma current. The origins of this increase, whether mainly β, mainly $l_i/2$ or both, are discussed in a companion paper [1]. Figure 1 illustrates the changes in $(\beta + l_i/2)$ when different R.F. power levels are applied, for a range of plasma currents and three excitation conditions (driving predominantly n=4, n=1 and n=2 waves). The increase in $(\beta + l_i/2)$ is largest for low plasma currents and most effective for the n=4 modes. Since, under our standard conditions, the n=4 resonance surfaces are in the outer part of the plasma, this result is at first sight surprising. This whole issue is further complicated by the substantial increase in density which occurs during the R.F. pulse.

In order to proceed further, we have studied the values of $(\beta + l_i/2)$ obtained in quasi-stationary ohmic discharges for three values of toroidal field (0.78, 1.16, 1.51 T) and plasma currents from 40-135 kA. The wide range of values obtained, Fig. 2a, can be reduced to an extremely good description of the density dependence by using the quantity $\Lambda^* \cdot (I_p/130\ \text{kA})$ where $\Lambda^* = (\beta + l_i/2 - 0.7)$. The value 0.7 was selected to give the least deviation in the data. This quantity does not itself appear to have any absolute merit. However, we can redraw Fig. 2b scaled by $1/B_\phi$ in which $\Lambda^* \cdot (I_p/130\ \text{kA}) \cdot (1.51\ \text{T}/B_\phi)$ is a well defined

function of $\overline{n_e}/B_\phi$, the Murakami parameter. That is to say the value of $\Lambda^*(\overline{n_e})$ divided by the value of β_p at the Troyon limit is determined by the fraction of the operational density range in ohmic conditions. The selected value 0.7 chosen to generate Λ^* corresponds to the minimum value of $(\beta + l_i/2)$ at high current (q_a=3), being roughly $l_i/2$ for q_a=3. At lower currents $(\beta + l_i/2 - 0.7)$ does not correspond to β, since the $l_i/2$ contribution is then larger (Fig. 1a).

When we look at non-stationary ohmic discharges, $(\beta + l_i/2)$ can be higher than predicted by the stationary scaling, for example during a rapid density ramp-up. An example is shown as a dashed line trajectory in Fig. 2b.

At the higher levels of R.F. power, the discharge evolution follows a much higher trajectory in the same plane and the maximum $(\beta + l_i/2)$ values achieved were shown in Fig. 1. Figure 2 shows the same results versus the plasma density and a certain alignment is already visible. With some hindsight we replot the data on the $\Lambda^* \cdot (I_p/130\ kA)$: $\overline{n_e}$ plane, Fig. 4, with a typical trajectory shown as a dashed line. The R.F. accessed region is way above the quasi-stationary ohmic scaling, and exceeds the trajectory for hard gas-puffing. The different plasma currents and excitation modes are now indistinguishable. The most noticeable feature is that the maximum $\Lambda^* \cdot (I_p/130\ kA)$ does not exceed the maximum ohmic value, that is, the ohmic value near the density limit ($\overline{n_e} \sim 8 \times 10^{19} m^{-3}$). At the lowest densities the effect of the R.F. is most marked, that is, when the ohmic discharge is "weakest".

The data shown in Fig. 4 are those obtained in pulses which did not disrupt. On trying to exceed this experimentally observed limit, a disruption will ensue, characterised by a progressive increase in the $B_{\theta a}(m=2)$ amplitude. This form of disruption is similar to the density limit disruption, but at a lower density, one at which there would be no significant m=2 activity in a quasi-stationary ohmic discharge. However, when we consider $\Lambda^* \cdot (I_p/130\ kA)$ as the determining parameter the phenomenology of the two types of disruption is similar, Fig. 5. The details of the excited spectrum are, however, important as already noted [2], and can systematically alter the dependence of Fig. 5, but not by very much. The observation that the disruptions are most likely to occur near a mode threshold corresponds to the observation that the highest point in the $\Lambda^* \cdot (I_p/130\ kA)$: $\overline{n_e}$ plane is also frequently close to a mode threshold.

The power levels in Fig. 1 (a,b,c) are much lower than the available R.F. power. It has always been considered that the n=2 excitation is preferable in that much more R.F. power can be delivered than for n=1, n=4. On reanalysing the highest power data, the trajectories of those shots do, nonetheless, lie within the distribution of Fig. 4. We had found a way of increasing the power acceptance in conditions in which the increase in $(\beta + l_i/2)$ had virtually saturated. In general, the longer R.F. pulses with lower ramp-rates produced less marked increases in $(\beta + l_i/2)$, and tolerated a greater level of R.F. power.

Discussion : These results show that all the quasi-stationary ohmic data can all be described by a simple law relating ($\beta + l_i/2$) to the Troyon limit and the Murakami factor for a given density. In this parameterisation, the maximum achieved ($\beta + l_i/2$) is simply studied for varying plasma conditions, and we find that, although we exceed the ohmic conditions for low density plasmas, we do not exceed the maximum value for $\overline{n_e}=8\times10^{19}m^{-3}$.

Acknowledgements : This work was partly funded by the Fonds National Suisse de la Recherche Scientifique.

References

[1] Th. Dudok de Wit at al., paper presented at this conference.
[2] K. Appert et al., 1987 Int. Conf. on Plasma Physics, Kiev, USSR, 1987. (LRP 321/87)

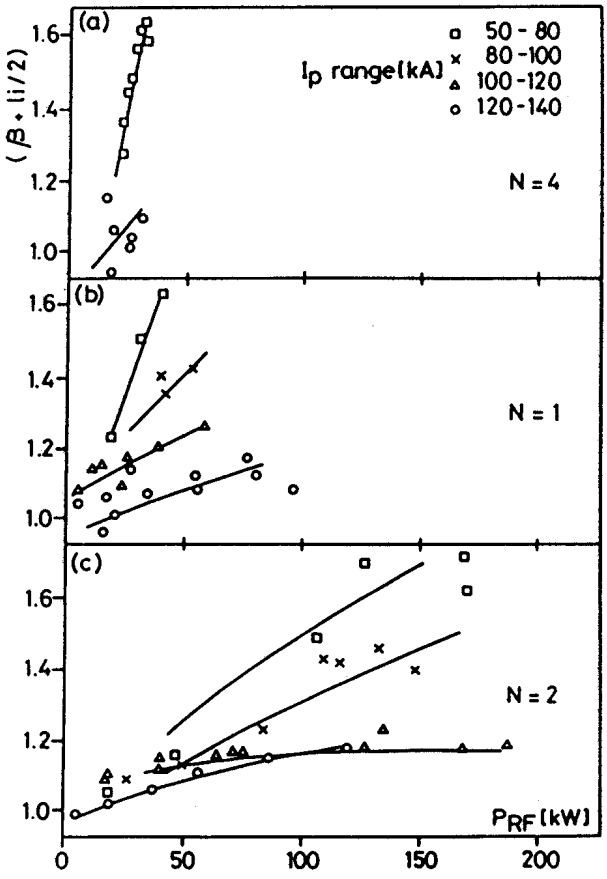

Fig. 1 ($\beta + l_i/2$) achieved as a function of both delivered R.F. power and plasma current for a) n=4 b) n=1 c) n=2 [B_ϕ=1.51 T, f=2.5 MHz, D_2].

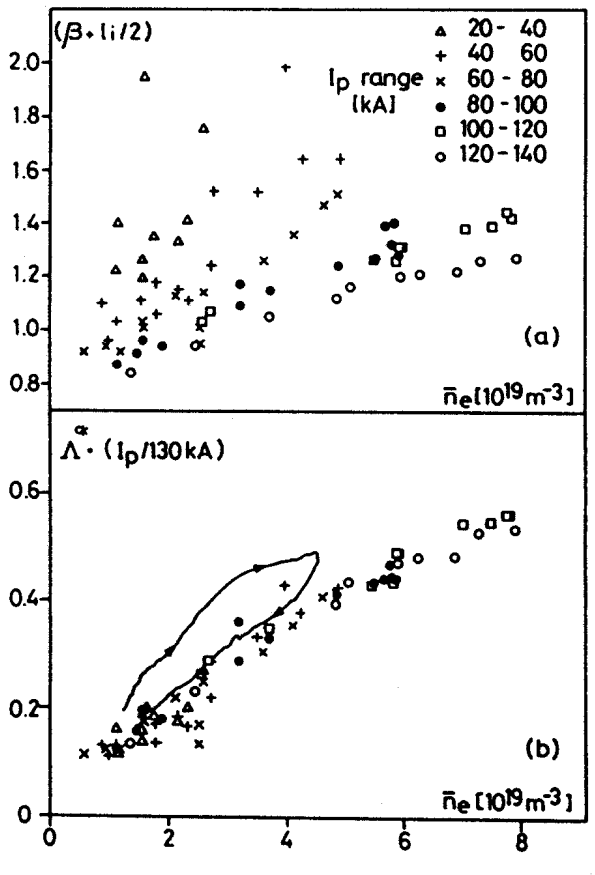

Fig. 2 a) ($\beta + l_i/2$) as a function of n_e for ohmic discharges with different plasma currents b) $\Lambda^* \cdot (I_p/130$ kA) for the same data [B_ϕ=0.78, 1.16, 1.51 T, D_2].

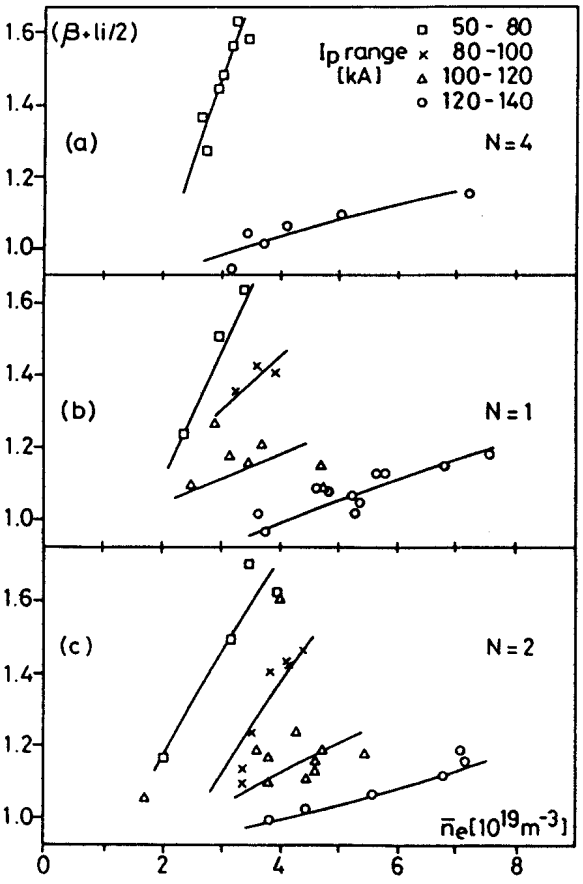

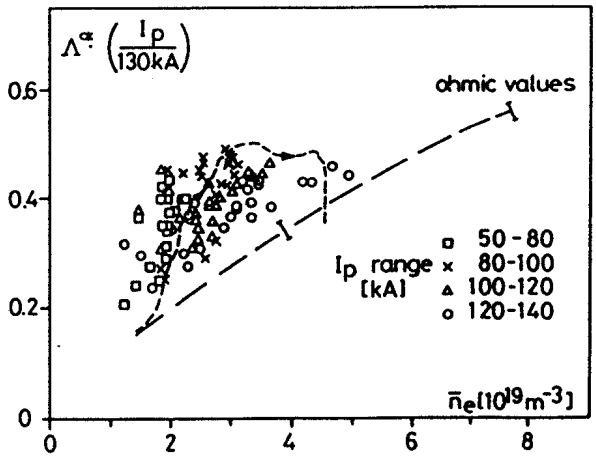

Fig. 4 R.F. discharges in the $\Lambda^* \cdot I_p$: $\bar{n}_e$ plane, for different plasma currents [B_ϕ=1.51 T, f=2.5 MHz, D_2].

Fig. 3 The data of Fig. 1 replotted as a function of the maximum density reached. ←

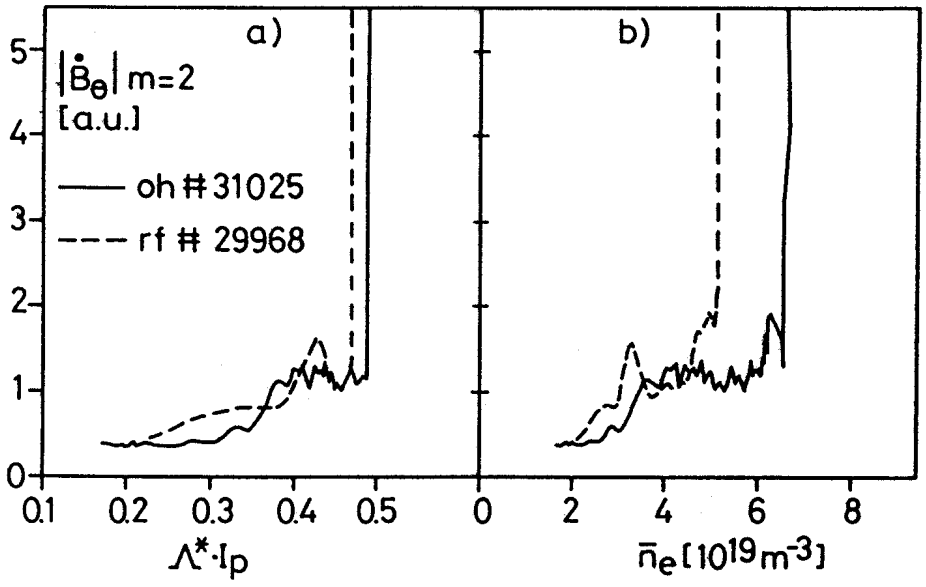

Fig. 5 Evolution of the m=2 amplitude as a function of a) $\Lambda^* \cdot I_p$ and b) $\bar{n}_e$ for ohmic and R.F. discharges.

ION TEMPERATURE EVOLUTION DURING ALFVEN WAVE HEATING IN TCA

A.de Chambrier, B.P.Duval, J.B.Lister, F.J.Mompeán* and J.-M.Moret

Centre de Recherches en Physique des Plasmas
Association Euratom - Confédération Suisse
E.P.F.L. Lausanne, Switzerland
* seconded from C.I.E.M.A.T., Madrid, Spain

ABSTRACT: The application of Alfvén Wave Heating, (AWH), is accompanied by an electron density (n_e) rise and an increase in the ion temperature, (T_i), measured with a Neutral Particle Analyser (NPA). A study was performed and a formula developed to model the T_i in non stationary ohmic discharges, to determine if the T_i increase is simply due to n_e. When compared with AWH discharges, the observed T_i is consistently higher than predicted by the ohmic model, indicating an additional source due to the RF. T_i also reflected the evolution of the AW spectra and reaches a maximum at the onset of a new continuum ie: when the resonant surfaces are in the outer half of the minor radius. T_i was investigated with modulated RF power, and a modulated gas puff, measuring the phase and amplitudes of the T_i rise relative to the perturbation. We conclude that the RF appears to have a direct effect on the T_i.

Introduction: The results described were obtained on the TCA tokamak (R, a = 0.61, 0.18m, I_p up to 170kA, B_ϕ up to 1.51T, Deuterium Plasma). T_i was measured with a five channel NPA obtained from the A.F.IOFFE Institute [1]. The installation, calibration, and operation of this spectrometer on TCA is described in detail by [2]. Additional RF heating was provided at a frequency of 2.0 - 2.5MHz with pulses up to 80msec long and delivered RF power up to 200kW. The details of the Alfvén Wave launching scheme are described in detail by [3] and a resumé of its application to TCA has been given by [4]. To recall the relevant features of this heating scheme, (N,M) are the toroidal and poloidal mode numbers of the exciting antennae structure and (n,m) are the mode numbers of the wave driven in the plasma. The RF energy is predicted to be damped by the electrons which have approximately the same thermal velocity as the Alfvén wave speed.

The RF pulse produces a rapid increase in ($\beta+l_i/2$), the soft X-ray flux, n_e (see Fig 1b), and the flux in the NPA channels. For certain plasma conditions, the T_i measured by the NPA increases significantly [2].

Ohmic Study: The understanding of T_i is complicated by the increasing n_e, so the plasma may not be considered quasi-stationary. As n_e increases, the power transfer rate from the increased electron-ion collisionality leads to a T_i increase. An early effort to estimate this indirect heating term [5] suggested that the increase in T_i was greater than expected simply from ne. The timescale of the n_e increase makes a quasi-stationary analysis inadequate, obliging us to consider terms depending on dn_e/dt and dT_i/dt. The increase in T_i is observed to saturate at both high I_p and n_e. This saturation may be explained by the reduction in the collisional transfer from the electrons, and here only discharges for which I_p was constant are

considered. The ion power balance can be simply written, valid for an ill-defined central region, as:

$$dW_i/dt = 3/2\, e\, (dT_i/dt\ n_e + T_i\, dn_e/dt) = P_{ei} - 3/2\, e\, T_i\ n_e/\tau_{ei}$$

where W_i is the power of the ions, and, for the moment, all losses have been lumped together using an energy confinement time τ_{ei}. An empirical form $\tau_{ei}(n_e) = C\, n_e^a$ was chosen to reproduce the quasi-stationary form of $T_i(n_e)$. Fig. 1a) shows the results of this fit together with the experimental n_e trace exhibiting excellent agreement with the experimental trace. By introducing impurity gas puffs, we concluded that an unsupportably high impurity contamination would be required to significantly alter this analysis.

T_i During RF Heating: Applying the RF pulse leads to an increase in all the NPA channel fluxes the estimated T_i. The measured neutral particle energy spectrum before, during and after an RF heating pulse remains Maxwellian. The T_i increase is largest when the pre-RF T_i was lowest, and rises linearly with RF power, and saturates with the large n_e increase. For a discharge with AWH, the T_i calculated the ohmic model, and the measured n_e, differs from the measured value, Fig.1b. T_i increases at the start of the RF pulse, instead of the decrease which would be predicted by $dW_i/dt = 0$, suggesting that the model is incomplete.

In order to "correct" the simulation we would need to change at least one of the terms in the ion power balance. We could:

1) Add a term labelled "Direct Ion Heating" for which there is no theoretical support.
2) Modify P_{ei} by an anormaly factor which switched on during the RF pulse.
3) Suddenly reduce the ion losses by increasing τ_{ei} during the RF pulse.
4) Assuming that the incoming plasma is convected at high temperature.

Since in our analysis T_i is the result of these terms, we can not distinguish between these possibilities. In conclusion, we see the presence of a term that has the effect of directly heating the ions which is not accounted for by our ohmic model.

Effect of the Excited Spectrum: In the previous section, we treated one specific RF excitation condition with toroidal mode number n=2. As n_e increases with RF, the excited spectrum changes [4]. From the assumption of an RF induced ion power balance term, we might expect some spectral RF dependence. Three main excitation structures were driven with M=1 [3], and Hydrogen and Deuterium working gas was used, thus changing the spectral condition. The increase in T_i can change at the threshold of a Discrete Alfvén Wave, (DAW), signalled by an increase in the antennae loading curves. The form of the n_e increase can also change at this point and the maximum T_i is no longer obtained at the maximum value of n_e.

Figure 2 plots the maximum values of T_i and n_e during the RF pulse, not necessarily obtained simultaneously, for discharges with the same initial n_e and a range of RF powers. As the maximum n_e increases roughly linearly, T_i tends to increase. The RF power at which n_e rose sufficiently to cross the next Alfvén Wave threshold is marked by a vertical arrow. In this example, above this critical power, the maximum achieved T_i actually decreases. This

shows that the increase in T_i can be a strong function of the position in the AW spectrum, and is most "efficient" before a new threshold which corresponds to the RF resonance layers being far out in the plasma edge. Once the threshold is crossed, the new resonance surface, which is most important, is near the plasma centre. This new surface appears to have less effect on T_i.

RF Modulation Discharges: The RF power was sinusoidally modulated at 100Hz and the phase and amplitude response of n_e and T_i investigated. The analysis considers the T_i response as the sum of the change in the electron-ion collisional term, the n_e modulation and a postulated "direct" heating term. The magnitude of the direct term deduced from this analysis was larger than the supplied RF power indicating that the model is quantitatively deficient. Interestingly, the phase of the T_i response relative to the RF power was observed to slide between two quasi-stationary values across the passage of a DAW, Fig. 3, which correlates with the discontinuity observed with continuous RF heating. In a similar comparison to that above, the response to a modulated gas puff was investigated. The modulation frequency was limited to 30Hz by the relatively slow response of n_e to the gas valve, but no phase slide, similar to that with RF, was found. The linear analysis of the gas puff modulation experiments could also be interpreted as an increase in the ion energy confinement, but smaller than that observed with the RF.

Conclusions: This paper investigates the reaction of the ion temperature to Alfvén Wave Heating. The analysis has been handicapped by the n_e rise associated with the RF, which requires that many time dependent terms be included in the ion power balance. The n_e rise was modelled by a time dependent ion loss term for an ohmic discharge with a gas puff induced n_e rise. The RF heating induced n_e rise did not agree with this model, which lead us to consider a direct effect of the RF on T_i. An attempt made to calculate this term using RF modulation experiments, although tending to confirm the need for such a term, gives a value with an unreasonably high magnitude. Since the n_e rise with Alfvén Heating is not yet understood, it could still be argued that this postulated term could be solely due to a difference in the dynamics of the RF and gas puff. This could not explain the discontinuities in the T_i behaviour coincident with strong spectral RF features like the DAW. We thus conclude that T_i is in some way directly influenced by the RF, although we can not identify the term responsible.

In preliminary results, the RF induced n_e rise is observed to saturate with time. Using this, and the recent prolongation of the plasma pulse on TCA, and the ability of our RF generator to give longer pulses we hope to be able to continue these experiments with more stationary plasma conditions.

Acknowledgment: We would like to thank all the members of the TCA team for the machine operation and diagnostic information. This work is partially supported by the Fonds National Suisse de la Recherche Scientifique.

References:

[1] AFROSIMOV V.V. et al. Sov. Phys. Tech. Phys. 20 1 (1975)
[2] de CHAMBRIER A. Doctoral thesis 712 EFPL/CRPP LRP 345/88 (1988)
[3] COLLINS G.A. et al. Plas. Phys. Fluid. 29 2260 (1986)
[4] BESSON G. et al. Plas. Phys. & Contr. Fus. 28 1291 (1986)
[5] BEHN R. et al. Plas. Phys. & Contr. Fus. 26 173 (1984)

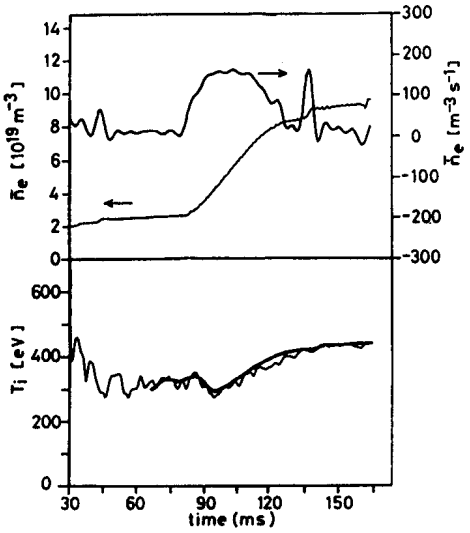

Fig 1a) ne and Ti for a discharge with a strong gas puff. The ohmic model fitted Ti is shown Bold

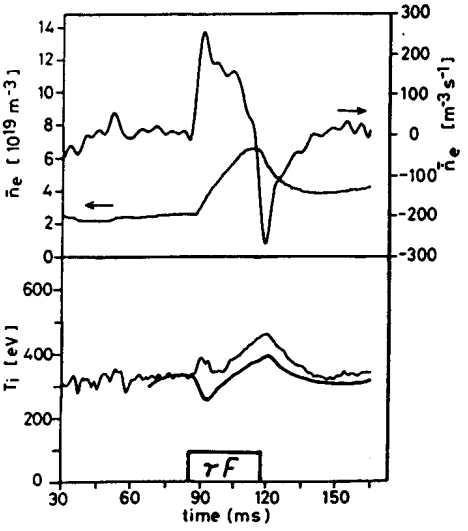

Fig 1b) As above, but for a Discharge with RF heating. The Ohmic model fit (Bold) is no longer in good agreement.

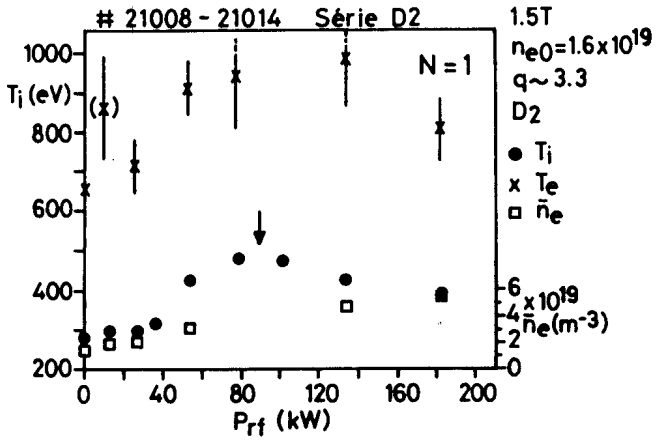

Fig 2) The maximum values of Ti and ne for a series of discharges with N=1 and the same initial density with a scan of RF power. The power at which the RF spectrum crosses a DAW is marked by a vertical arrow.

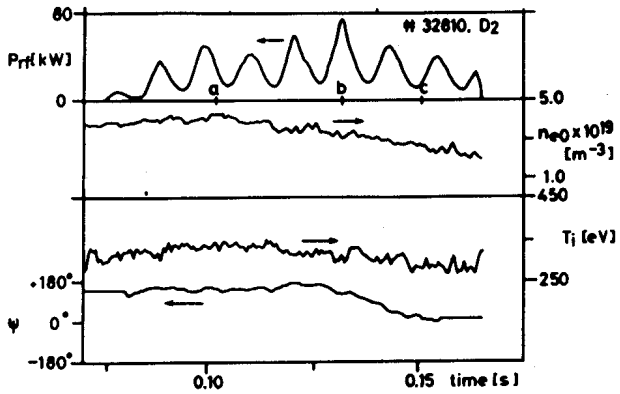

Fig 3) RF modulation experiment showing the deduced n_e and T_i. The phase of the T_i modulation relative to the RF is shown. As ne drops, there is DAW resonance, across which the phase is seen to change between two quasi-stationary values.

INFLUENCE OF THE ALFVEN WAVE SPECTRUM ON THE SCRAPE-OFF LAYER OF THE TCA TOKAMAK.

Y. Martin, Ch. Hollenstein.

Centre de Recherches en Physique des Plasmas
Association Euratom - Confédération Suisse
Ecole Polytechnique Fédérale de Lausanne
CH-1007 Lausanne / Switzerland

Abstract The study of the Scrape-Off Layer (SOL) during Alfvén wave heating may lead to a better understanding of the antenna - plasma interaction. The SOL of the TCA tokamak has been widely investigated by means of Langmuir probes [1,2]. The aim of the present work is to present in detail the influence of the Alfvén wave spectrum on the SOL. The experiments have shown that the plasma boundary layer is strongly affected by the RF, in particular the ion density, the electron temperature and the floating potential. In TCA, as the spectrum evolves due to a density rise, the passage of the Alfvén continua and their associated eigenmodes (DAW) induces a strong depletion in the edge density of up to 70 % during the continuum part and a density increase during the crossing of an eigenmode. The floating potential becomes negative during the continua and even more negative crossing the eigenmodes. This behaviour changes as a function of the power transmitted to the plasma through the antennae, especially we have found with MHD modes a change around 100 kW. The profiles of the basic parameters are modified, depending on the wave spectrum. MHD mode activity which can occur during the RF phase considerably alters the behaviour mentioned above. Finally, the modulation of the RF power allows us to characterize the difference in coupling, for the continua and the eigenmodes, between the Alfvén wave field and the scrape-off layer.

INTRODUCTION The antennae for additional heating are always placed in the scrape-off layer of tokamaks. Thus, the plasma boundary strongly interacts with the wave field and, moreover, the behaviour of this boundary plasma could be connected with the efficiency of the wave heating. Therefore a good knowledge of the plasma boundary can help the understanding of the coupling between the wave and the core plasma. To analyse the scrape-off layer we used Langmuir probes which give information on its principal characteristics such as ion density, plasma potential and electron temperature. One aim of the TCA Tokamak being the study of the Alfvén Wave Heating (AWH), we present here the influence of the RF wave field on the scrape-off parameters.

EXPERIMENT The TCA is a medium sized tokamak with the following parameters: $R = 0.61$ m, $a = 0.18$ m, $B_\varphi \leq 1.5$ T. The working gas was H_2 or D_2 with currents of up to 130 kA, which gave a safety factor at the edge greater than 3.

The RF wave field is produced by eight groups of antennae regularly spaced around the torus, four on the top and four on the bottom, three centimeters away from the plasma.

The Langmuir probes are located in the outer equatorial midplane toroidally opposite to the limiter. The four probes can be moved radially in the plasma boundary. They are made of Molybdenum wire and measure 5 mm long and 0.5 mm diameter with 5 mm between them to form a square. Two of these serve to measure the ion density (absolute and

fluctuations) by the means of a current probe with a frequency bandwidth from DC to 50 MHz. Another gives the floating potential in a frequency range of DC to 20 MHz, and with the last one, swept from -130 V to 80 V in 1 ms, we can have a rapid calculation of the electron temperature.

RESULTS Using periodic cylindrical geometry to describe the toroidal plasma, the Alfvén wave can be excited with the following dispersion relation where ω is a function of the radius via the mass density and the safety factor:

$$\omega^2(r) = \left(\frac{1}{R_0}\right)^2 \left(n + {}^{m}/_{q(r)}\right)^2 \frac{B_0^2}{\mu_0\ \rho(r)} \left(1 - \frac{\omega^2}{\omega_{ci}^2}\right)$$

with n and m the toroidal and poloidal mode numbers. When a density rise occurs, according to the MHD theory, shear Alfvén waves (continua) are generated in the centre and move towards the edge. Besides that, we observe global eigenmodes (DAW) which are the low frequency counterpart of the ion cyclotron wave. These modes are superimposed on the continua and give the spectrum as shown in the previous papers on Alfvén waves in TCA [3]. In the scrape-off layer, the Alfvén wave field yields a strong perturbation in the ion density and in the floating potential. Firstly, when a shear Alfvén wave appears, the ion density decreases very rapidly and stays at this low level (down to 30 % of the Ohmic value) during all the presence of this mode (fig. 1). During this time, the floating potential decreases regularly and becomes very negative (-30 Volts). As a global mode enters the plasma, the density increases and reaches a value often higher than that of the Ohmic value. The floating potential becomes still more negative (up to -60 Volts).

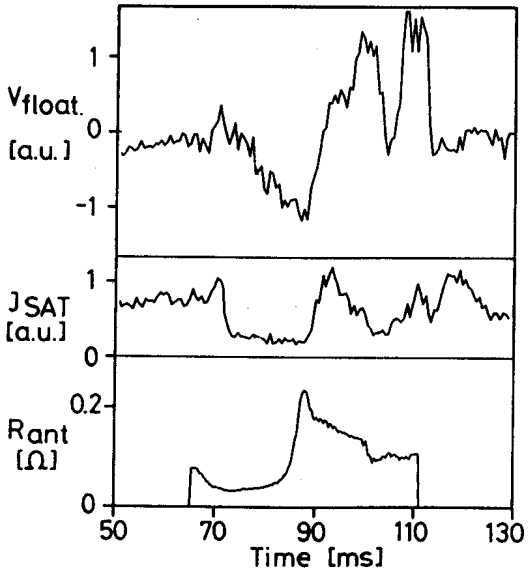

Fig. 1.

This behaviour is clearly seen in front of the antennae where the influence of the wave field is the strongest (fig 2). During the continua, in case of mode activity, the edge density rises. This explain the two curves on fig 2. Behind the antennae, which are also limiters in a way, the density is very low and the plasma interacts only slightly with the wave.

Looking more precisely on the loading curve, we can observe, just after the passage of a global mode, some small oscillations [4], which are also revealed with high sensitivity in our data.

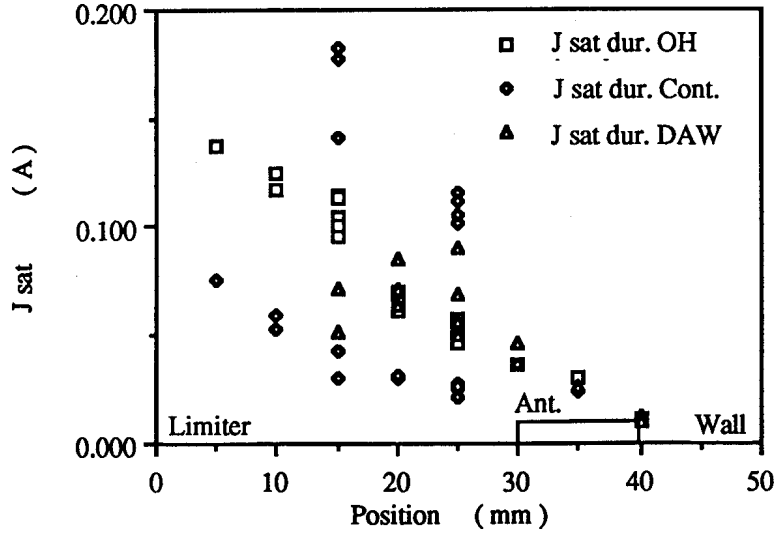

Fig. 2.

It is known that the presence of MHD mode activity usually increases the density in the scrape-off layer. In TCA we observe this phenomenon in Ohmic conditions. When Alfvén waves are injected, we find that, for an RF power greater than 100 kW, the mode activity is too strongly established so the decrease of the density does not occur, but the density goes up continuously. For smaller powers ($\leq$ 100 kW), the density decreases and the mode activity stops. In figure 3 we show the difference of the density taken at two times in the RF pulse as a function of the power delivered to the antennae.

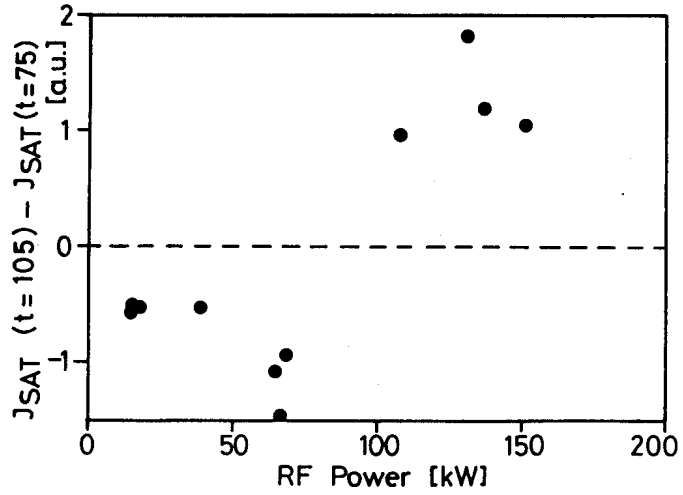

Fig. 3.

For the shots without any modes, we have shown the density and the floating potential as a function of the power delivered to the antennae (fig 4). The aim of this measurement was to verify a model which would explain the dependence of the loading on the RF power.

According to this model, the scrape-off layer, interacting with the local wave field of the antennae provides a sink for the direct dissipation of the antenna current [5]. When the RF power increases, the scrape-off layer is swept away and changes the antenna loading. The behaviour of the density agrees with this model. Our experiment however needs a more complete set of data on a wider range of power.

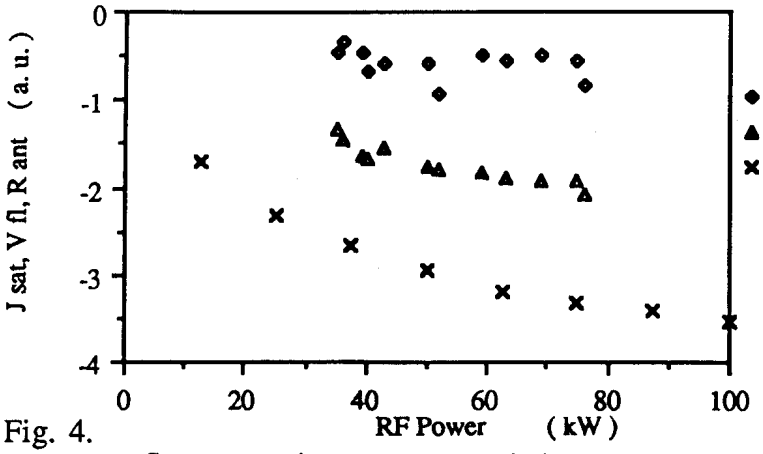

Fig. 4.

Some experiments were carried out on the tokamak to study the dynamic response of the plasma [6]. The RF power can be modulated. In this case, the modulation was fixed at 500 Hz and the peak to peak amplitude was almost twice the usual mean value. A calculation provides the gain and the phase of the transfer function from the input trace (RF power) to the output trace (J sat) as shown in the figure 5. We can see the difference of the gain between the continua and the discrete mode. This means that there is a strong interaction between the wave field and the scrape-off layer during the continua so we can say that a non-negligible part of the energy is deposited in the plasma boundary. When a global mode enters the plasma the coupling is more efficient with the bulk plasma and the energy is better deposited in the plasma core.

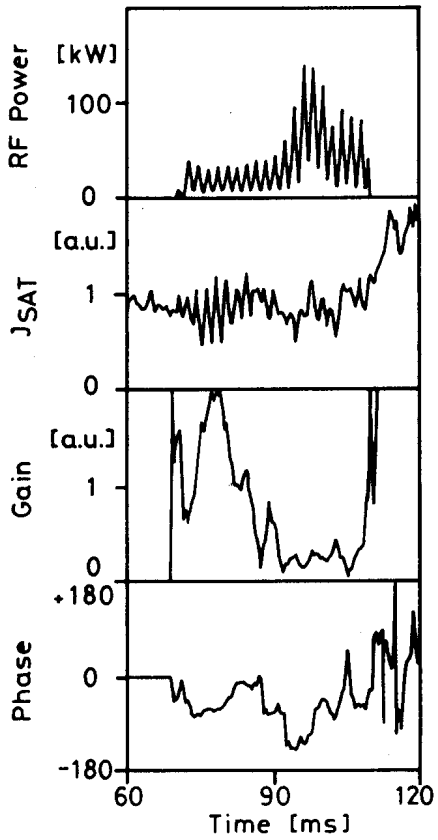

Fig. 5.

CONCLUSION All the measurements reveal a strong interaction between the wave field and the scrape-off layer. We show the difference of the behaviour of the plasma boundary especially when the spectrum of the wave field evolves. We find an important decrease of the edge density due to RF power deposited which could lead to a decrease of the impurity transport. The RF power seems to be more deposited in the plasma boundary during the continua. The boundary plasma density can be very strongly modified by the RF power, the modulation of the RF power and the mode activity.

ACKNOWLEDGEMENTS We wish to thank the whole TCA team for its excellent support. The present work was partially supported by the Fond National Suisse de la Recherche Scientifique.

REFERENCES [1] A. de Chambrier et al. J. Nucl. Mater. 128 & 129 (1984) 310.
[2] Ch. Hollenstein et al.: Proc XII EPS Conf. Contr. Fus. Plasma Phys. (Budapest 1985) vol. II p. 601.
[3] G. Besson et al. in: Plasma Phys.and Contr. Fus. (1986) Vol 28 no 9A p. 1291.
[4] K. Appert et al. in: Int. Conf. Plasma Phys. (Kiev 1987).
[5] G.A. Collins et al. Phys. Fluids 29 (7) July 1986 p. 2260.
[6] B. Joye et al. Dynamical plasma response to additionnal heating. Accepted for publication in Plasma Phys. and Contr. Fus. 1988.

MAGNETIC MEASUREMENTS OF THE SAWTOOTH INSTABILITY IN JET

P.A. Duperrex[1], A. Pochelon[1], A. Edwards, R. Granetz, J. Snipes

JET Joint Undertaking, Abingdon, Oxon, UK
[1]CRPP/EPFL, 21, Av. des Bains, CH-1007 Lausanne, Switzerland

Abstract : Magnetic coil signals are used to obtain the toroidal mode number spectrum of the sawtooth instability in a small-aspect-ratio tokamak. The excellent correlation between the edge (magnetic) displacement and the core displacement (soft X-ray tomography) demonstrates the validity of this approach and makes magnetic coil measurements an appropriate tool for studying the sawtooth instability global wavefunction.

Introduction : We have shown earlier that the sawtooth crash is accompanied by a simultaneous magnetic spike, which has been called the "gong" mode [1, 2]. Although the physical nature of this magnetic perturbation was not fully established, it was used to characterize the sawtooth instability. Toroidal mode number analysis, performed then with 4 equally spaced coils yielded a dominance of the n = 1 mode, with some 20-30 % of n = 2. The gong mode was shown to be particularly strong at the low field side midplane. Typical growthrates in the range of $\gamma \sim 10^4 s^{-1}$ were found to compare well with the typical sawtooth collapse times [3]. The sign of the mode's helicity was shown to be identical to the field lines' helicity. These observations showed that the magnetic perturbation was intimately related to the sawtooth instability in the core. In this paper we show a detailed comparison of the gong with soft X-ray tomography. The toroidal mode number spectrum evolution is obtained from 8 equally spaced coils, which allows us to follow the n-spectrum from n=0 to 4.

Plasma displacement : To show the evidence that the gong is in fact a direct measurement of the sawtooth instability, we had to find a parameter which could be measured independently by the soft X-ray diagnostics and the magnetic pick-up coils. The appropriate parameter for comparison was found to be the radial plasma displacement associated with the sawtooth instability. The m = 1 core displacement is accurately represented by the first moment of the soft X-ray emission profile F, which components $X_i = \int x_i F(x_1, x_2) dx_1 dx_2 \; / \; \int F(x_1, x_2) dx_1 dx_2$ define the centroid [4]. The centroid shift is then $\xi_{sx} = ((x_1 - x_1')^2 + (x_2 - x_2')^2)^{1/2}$, where the primed symbols refer to the position before the growth of the instability.

An estimate of the edge displacement can be made from the value of the poloidal field perturbation, as $\underline{b} = \underline{\nabla} \times (\underline{\xi} \times \underline{B}_0)$ in ideal MHD. In the cylindrical approximation the edge radial displacement can be expressed by $\xi(a) = (b_\theta(w)/B_\theta(a))\,(w/2m)\,(1 + nq/m)^{-1}\,[(w/a)^m - (a/w)^m]$ where a and w are the plasma and wall radius, m and n the poloidal and toroidal mode numbers of the gong. The edge displacement, which is directly proportional to the gong perturbation, can be analyzed for each n-component. As the main component of the gong was shown to be n=1, we will compare $\xi_{n=1}(a)$ with the centroid shift. This yields edge displacements $\xi_{n=1}(a)$ in the 10^{-3}m range. We note that gong-like perturbations in the ion saturation current are equally measured on a limiter langmuir probe. The ratio of edge n = 1 displacement to core displacement yields in the case of Fig. 1: $\xi_{n=1}(a)/\xi_{sx} \sim 3.10^{-2}$ with $q_\psi = 4.7$ and $b/a = 1.54$.

The fast rise of the instability is observed to start some 300 μs before the central soft X-ray emission drop (Fig. 1a). Both displacements exhibit the same temporal behaviour and the two traces overlap almost exactly, as shown in Fig. 1b. The agreement is maintained over the whole growth period and while the value of $b_{\theta n=1}$ is large. This demonstrates that the gong is directly linked with the sawtooth instability. The discrepancy between the two displacements noticed in the later phase following the temperature collapse, will be explained in the next section. Apart from this restriction which only applies to the second phase, the good agreement between edge and core information shows that the gong and the sawtooth instability form one single global n=1 motion. The absence of any phase lag between the edge and the core is typical of a single element oscillating system, which is related to the nature of toroidal coupling. An interesting corollary of this good agreement is the demonstration that the soft X-rays represent a good monitor of the magnetic surfaces, at least during the growth of the instability. Most importantly, the global properties of the sawtooth instability allow the use of the gong as an additional tool for studying the internal disruption instability.

Toroidal spectrum evolution : The toroidal spectrum contains important information related to the nature of the sawtooth instability. We have therefore extended the measurements to a toroidal array of eight equally spaced coils. Fig. 2a shows the eight integrated $\dot{b}_\theta$ traces, from which the n = 0, 1, 2, 3 and cosine n = 4 components are calculated. We first note that the n = 1, 2 and 3 modes all grow proportional to each other and seem therefore to belong to the same general motion. There is a nearly imperceptible n = 4 component, which suggests that the eight coils used are sufficient to qualify the n-spectrum of a sawtooth instability during the growth phase and in the case of JET. Some higher n perturbations may be present during the later profile reorganisation phase, after the saturation of the n=1 mode, as is suggested by Fig. 2b.

The n = 0 mode is related to the inward Shafranov-shift (reduction of poloidal field on all low field side coils, Fig.2a) following a reduction in $\lambda = \beta_p + l_i/2$. The n=0 trace evolves like the integrated n≥1 traces. Thus, the profile modifications seem to be a direct consequence of the n≥1 instability. The n = 0 growth rate, which is only slightly

smaller than the n = 1 instability growth rate, indicates that the λ changes occur on the same characteristic time scale.

The presence of this n=0 component is sufficient to explain the discrepancy mentioned in section 2 between $b_{\theta n=1}$ and ξ_{sx} following the sawtooth collapse. While $b_{\theta n=1}$ monitors a non-local toroidal component, ξ_{sx} on the contrary only measures the m=1 displacement in one specific poloidal plane. As a consequence, all the n-components contribute to ξ_{sx}, including the n=0 Shafranov shift in the late phase.

The decay index α of the n-spectrum of the instability, defined as $S(n) \cong A_1 n^{-\alpha}$ for $1 \leq n \leq 3$, yields a value of α of 2.5 ± 0.5. The most obvious way to interpret the n-spectrum is to assume that its measurement at the edge represents the n-spectrum on the q = 1 surface, therefore equivalently the m-spectrum on the q = 1 surface, as m = nq on a rational surface. Although the contribution from other surfaces cannot be excluded a priori, the fact that the fast gong-like changes observed on the soft X-ray chords are dominant within or close to the sawtooth inversion radius further support the core origin of the n-spectrum measured. However, the question must be posed whether departures from axisymmetry or whether non-linear mechanisms play a role by spreading the n-spectrum. Firstly, only gongs with vanishingly small superimposed helical Mirnov perturbations have been retained for analysis, as Mirnov oscillations not only destroy axisymmetry, but also directly pollute the measured n-spectrum. Secondly, very large amplitude gongs ($2.10^{-3} < b_{\theta n=1} < 7.10^{-3}$ T) may even show a reduced n = 2 component during the growth phase, whereas non-linear effects would show the opposite trend. Both these statements therefore support the thesis of the core origin of the n-spectrum for the presented cases. As a consequence, the n-spectrum may directly represent the m-spectrum on the q = 1 surface. Finally, and for normal sawteeth, the measurements indicate in addition to the n=1 mode non negligible n=m>1 mode contributions, growing all in parallel, which is not inconsistent with an interchange mode.

In an attempt to find scaling laws for the growth rate (measured at half maximum amplitude), we note that no trend is obtained for the growth rate as a function of external control parameters. The reason appears evident when considering that two consecutive gongs may show growth rate scattering as much as half an order of magnitude. Let us note that the use of Fourier components enables the measurement to be independent of plasma rotation. This shows therefore that the growth rate is controlled by details of the profiles. The growth rate is, however, found to be grossly proportional to the gong amplitude $b_{\theta n=1}$.

Conclusion : The gong mode has allowed us to measure characteristics of the sawtooth instability. Indirect experimental evidence indicates that the measured magnetic n-spectrum may be interpreted as an image of the m-spectrum on the q=1 surface. The n-spectrum, measured up to n=4, therefore indicates that the sawtooth instability has the characteristic behaviour of an interchange mode.

Acknowledgement : This work was partly funded by the Fonds National Suisse de la Recherche Scientifique.

References

[1] P.A. Duperrex et al., Helvetica Physica Acta 58 (1985) 85.

[2] P.A. Duperrex et al., EPS Conf. on Contr. Fus. and Plasma Phys., Vol.9F, I (1985) 130.

[3] A. Edwards et al., Phys. Rev. Lett 57 (1986) 210.

[4] R.S. Granetz et al., ibid [2], Vol. 11D, III (1987) 1256.

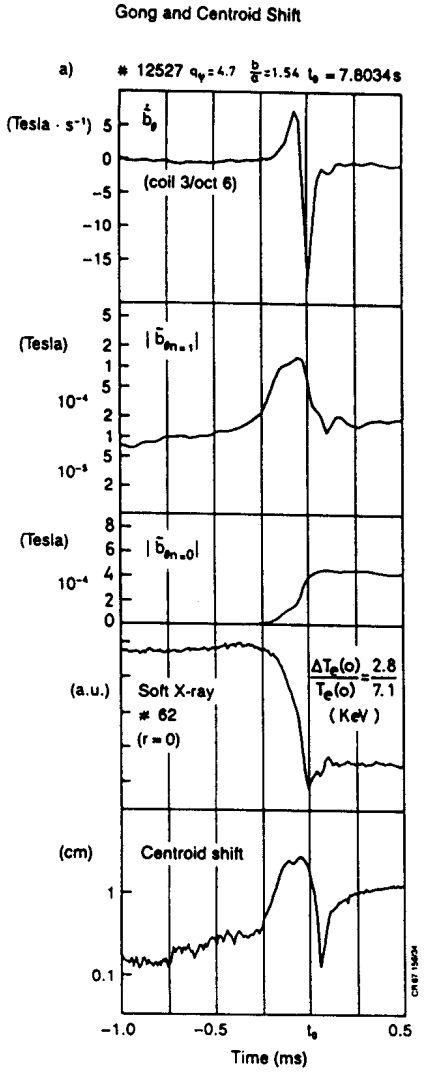

Fig. 1a)

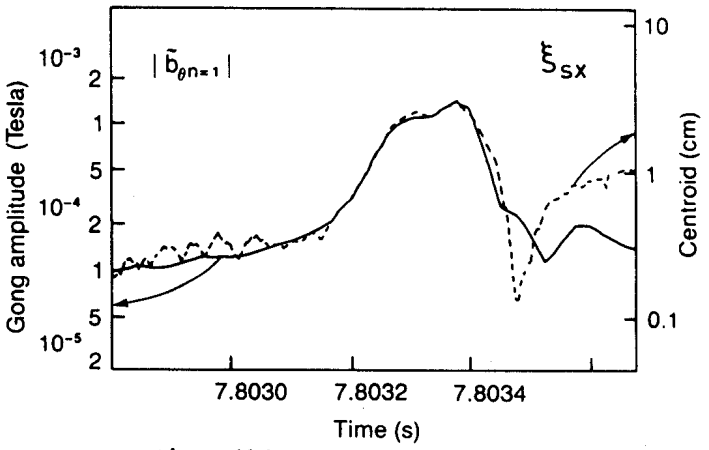

Fig. 1b)

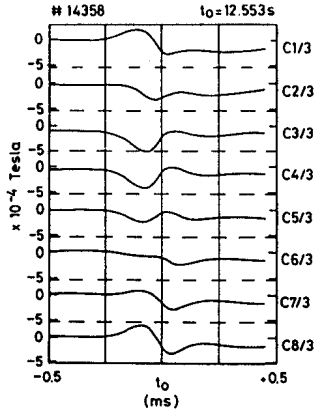

Fig. 2a)

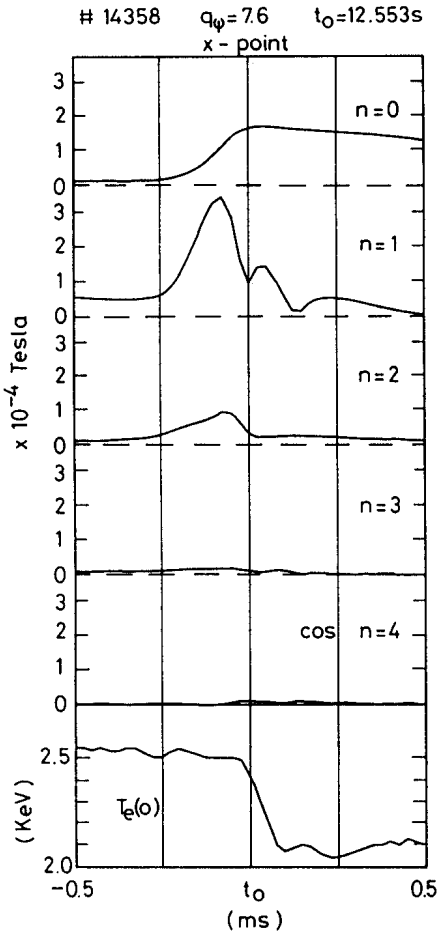

Fig. 2b)

Fig. 1 : The n=1 gong and m=1 centroid shift overlap

Fig. 2 : 8-coil toroidal spectrum analysis a) the integrated coil signals b) n-spectrum evolution

SIMULATION OF PLASMA CONTROL IN THE TCV TOKAMAK WITH HIGH FREQUENCY STABILIZATION

E.B. Marcus, F. Hofmann, S.C. Jardin*, R. Keller, J.B. Lister,
Ph. Marmillod, A. Perez, G. Tonetti

Centre de Recherche en Physique des Plasmas
Association Euratom - Confédération Suisse
Ecole Ploytechnique Fédérale de Lausanne
21, Av. des Bains, CH-1007 Lausanne / Switzerland

*Plasma Physics Laboratory, Princeton University,
Princeton, N.J. 08544, U.S.A.

Abstract :

The Tokamak Simulation Code (TSC) is used to study evolution, control, and growth rates of resistive, axisymmetric instabilities in the TCV (Tokamak à Configuration Variable). TCV is currently under construction. Its parameters are: B=1.43 T, R=0.87 m, a=0.24 m, b/a up to 3/1, Ip up to 1200 kAmp. The axisymmetric resistive growth rate is calculated for various equilibria passively stabilized by the TCV vacuum vessel. There exists a range of plasmas which are ideally stable, but which have resistive growth rates greater than those which can be controlled with 100 Hz, 12 pulse thyristor power supplies. We are able to control these high growth rate plasmas by producing a fast, relatively low power radial flux using coils inside the vacuum vessel. Detailed TSC evolutions showing the response of the plasma to these combined control and shaping coils are presented.

Introduction:

It has been demonstrated (1,2) with the Tokamak Simulation Code TSC (3) that a plasma in the TCV Tokamak can be evolved from a near-circular shape to a highly elongated plasma with a relatively broad current profile. Because of the limited bandwidth and voltage of the thyristor shaping power supplies and vessel attenuation, plasmas with peaked current profiles and high elongation having growth rates above 1000 / sec for the axisymmetric resistive vertical instability cannot be controlled. A wide range of highly elongated plasmas with peaked profiles are ideally stable(2), but they have resistive growth rates in the range 1000 - 5000 / sec, which is much larger than the inverse of the vessel time constant of 6.7 msec. We investigate methods of extending the operation range to include plasmas with peaked current profiles.

Fast Stabilization Coils :

A plasma is stabilized against vertical motion by image currents induced in the vacuum vessel. The resistive decay of these currents, and hence the loss of stabilizing flux, causes vertical resistive instability. The role of the active coil system is to provide supplementary flux so as to maintain the plasma at its desired position. In order to achieve this, we consider using additional coils inside the vessel in the region near the outer vessel corners and compare the results with using coils outside the vessel. The coils are placed in the corners (Fig. 4) to reduce interference with the plasma inside the vessel.

Results:

--The vacuum radial flux produced by a square voltage pulse of a given amplitude and 0.2 msec duration is an order of magnitude larger, for coils inside the vessel compared with coils outside. The flux produced by the inside coils is proportional to the linearly increasing coil current.
--With coils inside the vessel, it has been demonstrated that it is possible to stabilize both a 2/1 Dee plasma in the upper half and a symmetric 3/1 Dee plasma, with growth rates in the range of 1000 to 5000 / sec. The plasmas are stable with no visible distortion. The interesting result is that even though the radial flux pattern of the corner coils is highly distorted by vessel image currents, and symmetric about the midplane, on the time scale of less than 1-2 msec, plasmas both symmetric and nonsymmetric about the midplane can be stabilized. Also, higher order axisymmetric modes are not observed to be dangerous on this time scale.
--We conclude that it is sufficient to compensate on average the lost radial flux due to wall resistivity with radial flux from local sources in the corners on this time scale. On longer time scales than 1 msec, the outer 16 shaping coils precisely maintain the plasma shape, and limit the power requirements on the inner coils, as shown below.

Examples:

As an example, we choose a 3/1 elongated Dee shaped plasma with B=1.43T, Ip=1200 kAmp, qlim/qaxis=3, plasma-wall gap=.04 m, growth rate of 3600 / sec, initially at rest. The applied coil voltage is proportional to a linear combination of the flux difference between two flux measurement points at the top and the bottom of the plasma and its time derivative, with P=400000 volts/weber-radian, D=80 volts-sec/weber-radian. The inside coils have a resistance of 0.005 ohms, and the power supplies for these coils are ideal amplifiers with a nonlinear limit of +-50 volts. This system limits the inside coil currents to +-10 kAmps at low frequency. The lower plasma boundary is commanded to move upwards at constant speed (0.02 m in 2 msec). The command velocity of 10 m/sec represents a very approximate upper limit for three types of occurences which can induce plasma motion: 1. normal programmed motion during evolution to high elongation, 2. vertical motion due to a sawtooth or minor internal disruption in a non up/down symmetric plasma, 3. fluctuations at high beta.

A simulation is made with only the inside coils active, and the outside shaping coils short-circuited (with shaping currents present), for an interval of 0.002 seconds. The voltage initially jumps to -50 volts due to the D term in the feedback, in order to start the plasma moving vertically. The coil current also goes negative. Once the plasma starts moving upwards at 10 m/sec, the voltage changes sign to restrain the plasma, which is trying to go vertically unstable. The current also changes sign. During the first msec, the plasma moves smoothly upwards, following the command. However, during the period 1.0 to 1.5 msec, the coil voltage reaches its maximum, +50 volts, but the coil current increase is limited by an L/R approach towards a maximum of 10 kAmp. After 1.5 msec, because of this saturation, the control of the plasma is lost, and the plasma moves upwards with a growth rate of 3600 / sec.

In order to avoid this saturation, it is necessary for the fast inside coils and the outer shaping coils to work together, with the outer coils providing control and limiting the inside coil currents on a time scale of greater than 1 msec. The method adopted gives the same voltage per turn for the fast upper coil (no. 17, Fig. 4) and the four upper, outer shaping coils (nos. 9-12). The negative of this voltage is applied to the fast lower coil (no. 17) and the four lower, outer shaping coils (nos. 13-16). By this method, since there are four times as many coils with a much lower resistance, the outer coils reduce the current required in the inner coils on the long time scale.

This result is shown in Figs 1-4. In Figs 1 and 3, the currents in coils 18 (inside) and 16 (outside) are shown. The applied voltage, which is the same for both coils, is given in Fig. 2. The evolution of the limiting flux surface of the plasma (expanded) and the coil and vessel geometry are shown in Fig. 4. The outside coils are activated at 0.2 msec, after the plasma has started moving. Apart from the turn-on transient (the outside coils have no voltage limit in these simulations), the voltage and current of the coils inside the vessel and the plasma position evolve for the first msec similarly to the previous case (inside coils only). However, after the first msec, the inside coil current and voltage reach a maximum and then decrease, while the current in the outer coils continues to increase, which is the desired effect. The plasma lower boundary evolves linearly as programmed, demonstarting that control of the plasma can be continuously maintained. The actual thyristor shaping supplies on the outside coils should be able to act similarly to the linear model used here on a 1-2 msec timescale. The behavior of the magnetic axis reflects the non-rigid nature of the plasma, since it initially moves upwards at the same speed as the plasma lower boundary, then moves more slowly, since the plasma is scraping off on the upper limiter.

Based on calculations of radial flux due to coils inside or outside the vessel, control by outside coils of high growth rate plasmas would require high bandwidth and unrealistically high voltages. As an example, repeating the above evolution simulation with only coils outside the vessel, the same PD coefficients and no voltage limit, large plasma oscillations and control voltages an order of magnitude larger than in Fig. 2 are produced. With limiting conditions of 50 volts per turn on coils just outside the vessel at the corners, the voltage saturates for long periods, and control is not achieved.

Conclusions:

It has been demonstrated that high growth rate plasmas can be controlled with a simple additional coil system with high frequency response and reduced power. Inside and outside coils can operate in different bandwidth regions, and therefore reduce the total power requirements.

References:

1) F.B. Marcus, S.C. Jardin and F. Hofmann, Phys. Rev. Lett. 55, 2289 (1985).

2) F. Hofmann, S.C. Jardin, F.B. Marcus, A. Perez, A.D. Turnbull, in Fusion Technology 1986, Vol. I, Commission of the European Communities (1986) 687.

3) S.C. Jardin, N. Pomphrey and J. DeLucia, J. Comput. Phys. 66 (1986) 481.

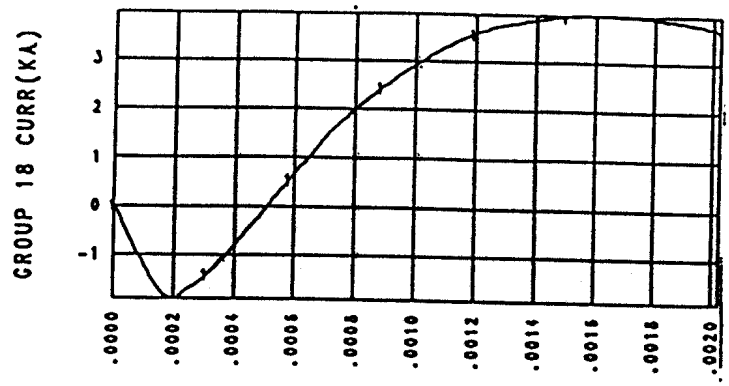

Fig. 1

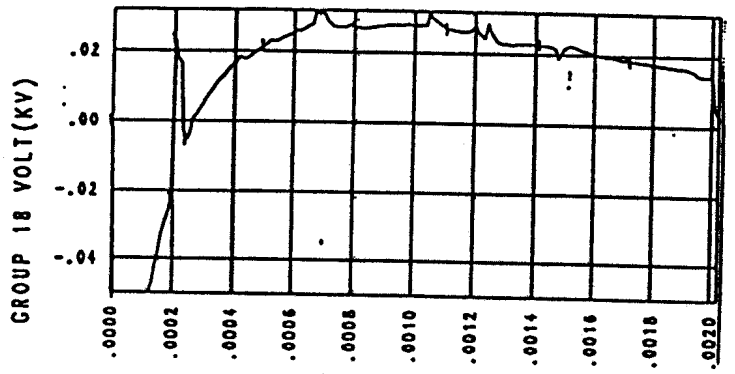

Fig. 2

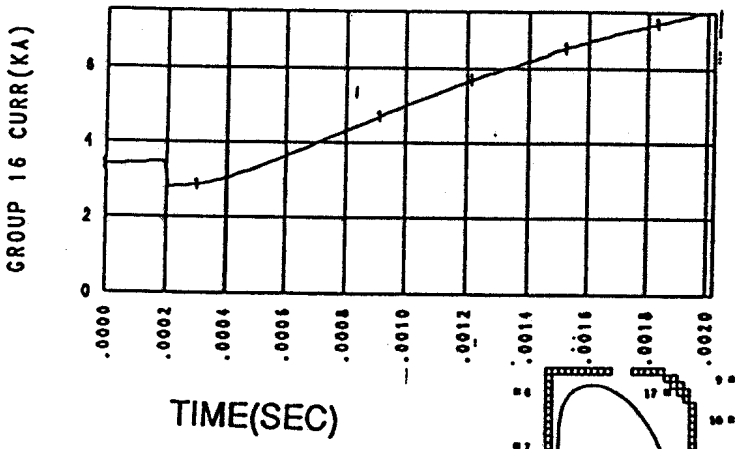

Fig. 3

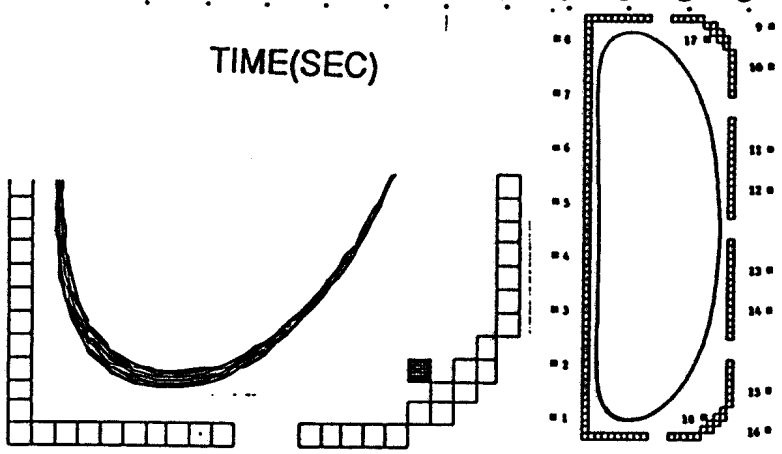

Fig. 4

Fig. 1-4. Controlled evolution of 3/1 elongated Dee shaped plasma, showing lower inside coil current and voltage, lower outside coil current, and evolution of limiting flux surface in TCV geometry.

INTEGRO-DIFFERENTIAL EQUATION APPROACH TO ELECTROSTATIC WAVE PROBLEMS IN ICRF

O. Sauter and J. Vaclavik

Centre de Recherches en Physique des Plasmas
Association Euratom - Confédération Suisse
Ecole Polytechnique Fédérale de Lausanne
21, Av. des Bains, CH-1007 Lausanne, Switzerland

Abstract

We solve the linear electrostatic wave equation for an inhomogeneous bounded plasma in an inhomogeneous magnetic field using a hot model valid to all orders in Larmor radius. This leads us to solving a homogeneous second order integro-differential equation with two boundary conditions. Thus we are able to find wave solutions, for any given density and temperature profiles, having wavelengths even smaller than the Larmor radius.

1. Introduction

The linear wave equations in the Ion Cyclotron Range of Frequency (ICRF) have been thoroughly studied using first cold models and then hot models. We are now able to solve the full electromagnetic 1-D problem, i.e. three components for the fields, using the hot model with an expansion in Larmor radius up to second order [1]. This implies a very complicated form for the dielectric tensor [2] and it would not be reasonable to go to third or higher orders, even though we can find cases where the second order expansion breaks down. Moreover Bernstein waves, which may have wavelengths comparable to Larmor radius, are not only important in the well-known mode conversion mechanism, but may also be used to heat the plasma via direct launching [3]. Therefore, there is a need for a hot model valid to all orders in Larmor radius.

2. Physical Problem

We study the electrostatic wave problem of an inhomogeneous bounded plasma in a slab geometry. The magnetic field is parallel to the z-axis and the plasma is inhomogeneous along x and extends from $x=x_{pl}$ to $x=x_{pr}$. We first solve Vlasov and Poisson equations in Fourier space [4]. As the plasma is bounded we have to transform back to real space, which is done by using the following integral representation of the modified Bessel function $I_j(z)$:

$$I_j(z) = \frac{1}{\pi} \int_0^{\pi} e^{z \cos\theta} \cos(j\theta)\, d\theta$$

3. Results

We shall present the results of an argon plasma. The typical parameters used are: $x_{pr}=-x_{pl}=3cm$; density: $n=10^{17}m^{-3}$; $k_z=100m^{-1}$; $B_o=0.2T$; $T_e=14eV$; $T_i=0.1eV$. The dispersion relation is shown in Fig. 1. We consider the region between the third and fourth harmonics. We take the sum over j in Eq. (2) between -10 and +10. Note that this summation is not time-consuming at all, enabling us to solve (1) at any harmonics.

We have chosen these parameters because the two branches are decoupled and because both waves have comparable amplitudes, which is not always the case. We shall change the magnetic field and the electron and ion temperature profiles illustrating the effect of the boundary, cyclotron damping and the influence on the wavelengths of the ion-acoustic and the Bernstein waves.

Let us first look at the dependence of the waves, in particular of their wavelengths, on the electron and ion temperature profiles. The ion acoustic wave is mainly affected by the electrons, whereas the Bernstein wave depends on the ions. This is clearly shown in Fig. 2 where we have an electron temperature profile going up from 2eV on the right hand side of the plasma (i.e. at the antenna) to 30eV on the left, and for the ions from 0.05eV to 0.5eV. This gives us, from the dispersion relation, wavelengths for the ion acoustic wave from 0.9cm to 3.7cm and for the Bernstein wave from 2mm to 6mm respectively. The wavelengths calculated from the solution, Fig. 2, follow well these variations, i.e. follow well the temperature profiles.

Modifying the value of the magnetic field allows us to change the ratio $\omega/\omega_{ci}=3.95$ at one edge to 3.60 at the other edge of the plasma. In the region where $\omega/\omega_{ci}=3.95$ we expect the Bernstein wave to be strongly damped. This explains why only the acoustic wave is emitted in the Low Field Side (LFS) case, Fig. 3a, whereas both waves are excited at the antenna in the HFS case, Fig. 3b. On the left plasma boundary, both waves can be reemitted. But due to the cyclotron damping mentioned above, the Bernstein wave can reappear only in the region $\omega/\omega_{ci}=3.60$, Fig. 3a.

Conclusion

We are able to solve the electrostatic wave equation in a 1-D inhomogeneous bounded plasma with hot plasma model valid to all orders in Larmor radius. Therefore, we can resolve consistently wave solutions having wavelengths even smaller than the Larmor radius.

References:

[1] K. Appert et al., in Proc. 7th Int. Conf. on Plasma Phys., Kiev 1987, Invited Papers.
[2] Th. Martin , J. Vaclavik, Helv. Phys. Acta 60 (1987) 471.
[3] M. Ono et al., Phys. Rev. Lett. 60 (1988) 294.
[4] F. Yasseen, J. Vaclavik, Phys. Fluids 26 (1983) 468.

Assuming a Maxwellian equilibrium distribution function and neglecting the electron Larmor radius and k_y, we get:

$$-\left(\left(1-\frac{\omega_{pe}^2\,\omega}{\omega_{ce}^2\,k_z v_{Te}}\,Z_{0e}\right)\Phi'(x)\right)' + \left(k_z^2+\frac{\left(1+\frac{\omega}{k_z v_{Te}}Z_{0e}\right)}{\lambda_{De}^2}\right)\Phi(x) \tag{1}$$

$$+\int_{x_{pl}}^{x_{pr}} K(x,x')\Phi(x')\,dx' = 0$$

with

$$K(x,x') = \frac{1}{2\pi^2}\sum_{\sigma}\sum_{j}\int_{x_{pl}}^{x_{pr}} dx'' \frac{\left(1+\frac{\omega}{k_z v_{T\sigma}}Z_{j\sigma}\right)}{\lambda_{D\sigma}^2\rho_\sigma^2}\,. \tag{2}$$

$$\int_0^\pi d\theta \frac{\cos(j\theta)}{\sin\theta}\exp\left(-\frac{(x-x')^2(1+\cos\theta)}{4\rho^2\sin^2\theta}\right)\exp\left(-\frac{\left(x''-\frac{x+x'}{2}\right)^2(1-\cos\theta)}{\rho^2\sin^2\theta}\right)$$

and $Z_{j\sigma} = Z(\omega - j\omega_{c\sigma}/k_z v_{T\sigma})$, where the subscript e stands for electrons and σ for ions species. ω_p, ω_c, v_T, λ_D are the plasma and cyclotron frequencies, thermal velocity and Debye length respectively. Z is the plasma dispersion function corresponding to the NRL formula.

We see that the kernel is symmetric and rather complicated. The theta-integral is singular at $\theta=0$, $x=x'$ and at $\theta=\pi$, $x''=(x+x')/2$. These singularities give a global singularity of the kernel $K(x,x')$ proportional to $\ln|x-x'|$, which is a weak and integrable singularity. But if we integrate over theta directly, the θ-singularities are proportional to $1/\theta$, which are not integrable numerically. Therefore, we have to do at least two integrations analytically or use special changes of variables. As we use a finite element method (with linear basis functions) to solve (1) numerically, we can manage to perform the integrations over x" and x' analytically. Thus we take care of both singularities and end up with a well-posed numerical problem.

We have chosen the following boundary conditions:

$$\Phi'(x_{pl}) = 0$$
$$\Phi'(x_{pr}) = -1$$

which means that we specify some surface charges simulating an antenna on the right plasma boundary.

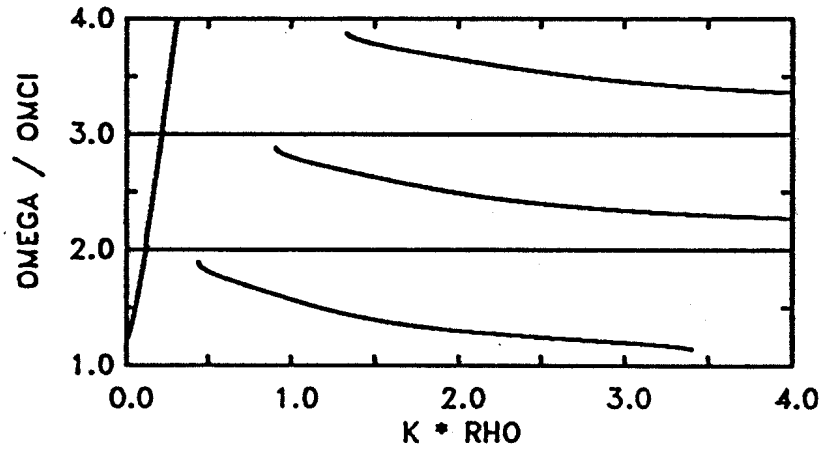

Fig. 1:
Dispersion relation, ω/ω_{ci} versus $k_x \cdot \rho_\sigma$, of the homogeneous argon plasma with ρ_σ=1mm.

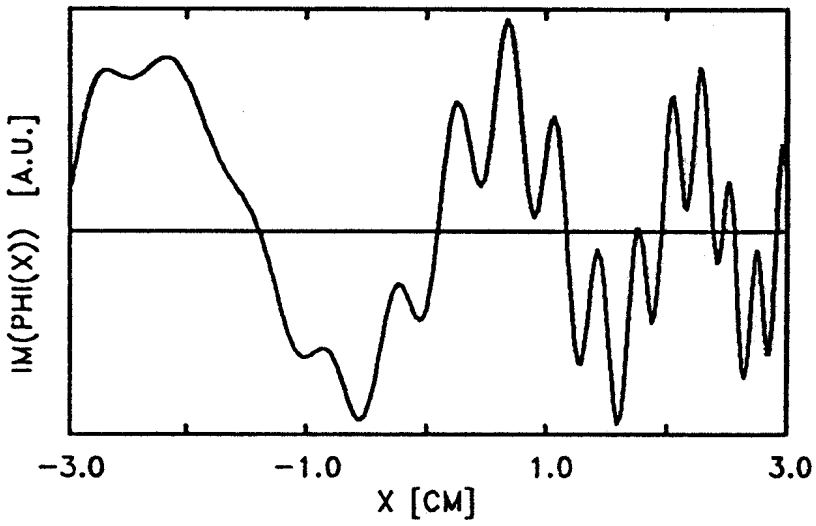

Fig. 2:
Imaginary part of solution $\Phi(x)$ versus x in the case of inhomogeneous electron and ion temperature profiles.

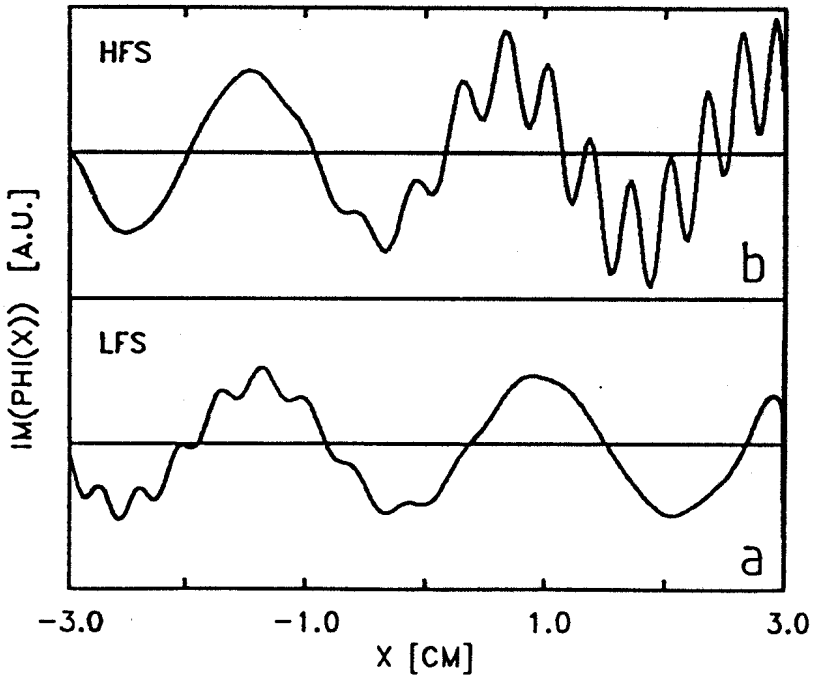

Fig. 3:
Imaginary part of $\Phi(x)$ versus x in the case of a inhomogeneous magnetic field, proportional to $1/(R_o \pm x)$, for LFS and HFS respectively. The same scale for both plots.

a) ω/ω_{ci}=3.60 at $x=x_{pl}$ and 3.95 at $x=x_{pr}$.

b) ω/ω_{ci}=3.95 at $x=x_{pl}$ and 3.60 at $x=x_{pr}$.

BALLOONING INSTABILITIES IN TOKAMAKS WITH SHEARED TOROIDAL FLOWS

W.A. Cooper

Centre de Recherches en Physique des Plasmas
Association Euratom - Confédération Suisse
Ecole Polytechnique Fédérale de Lausanne
21, Av. des Bains, CH-1007 Lausanne, Switzerland

The use of unbalanced neutral beam injection has induced toroidal plasma rotation that approaches the sound speed in TFTR [1] and in JET [2]. The toroidal rotation profiles measured in the TFTR device also display a significant amount of velocity shear [1]. Because ballooning instabilities can impose a limit on the beta (β) value that can be achieved in Tokamak devices, it is important to determine what impact plasma rotation and velocity shear can have on the stability properties of the plasma. Previous theoretical studies of ballooning modes in toroidal devices have suggested that the ballooning mode formalism described either through Weyl sequences [3] or with the covering space concept [4] breaks down when the velocity shear in the toroidal flow is finite [5]. In this work, the covering space concept is employed to represent ballooning mode structures that vary slowly along the magnetic field lines but rapidly across them. This eikonal ballooning representation is applied to the linearised magnetohydrodynamic (MHD) equations in axisymmetric systems with toroidal mass flows. In order to resolve the $\underline{V}\cdot\underline{\nabla}$ operator acting on perturbed quantities in a toroidal device, the eikonal function S must satisfy not only the usual ballooning condition $\underline{B}\cdot\underline{\nabla}S=0$ but also the condition $dS/dt=0$. This entails a Doppler in S, which in the PEST-1 magnetic flux coordinate system (s,θ,ϕ) with straight field lines becomes $S=\phi-q(s)\theta-\Omega(s)t+k(s)$. The surface functions q, Ω, and k correspond to the safety factor, the plasma rotation frequency and the radial wave number, respectively. The resulting set of initial value ballooning mode equations are:

$$\frac{\partial b_\perp}{\partial t} = -\left[n^2\eta|\underline{\nabla}S|^2 + \frac{2(\underline{\nabla}S\cdot\underline{\nabla})(\underline{V}\cdot\underline{\nabla}S)}{|\underline{\nabla}S|^2}\right]b_\perp + \frac{|\underline{\nabla}S|^2}{B^2}(\underline{B}\cdot\underline{\nabla})v_\perp$$

$$\rho_M|\underline{\nabla}S|^2\frac{\partial v_\perp}{\partial t} = \rho_M[2(\underline{\nabla}S\cdot\underline{\nabla})(\underline{V}\cdot\underline{\nabla}S)]v_\perp + B^2(\underline{B}\cdot\underline{\nabla})b_\perp - 2(\underline{B}\times\underline{\nabla}S\cdot\underline{\kappa})p$$

$$- [\underline{B}\times\underline{\nabla}S\cdot(\underline{V}\cdot\underline{\nabla})\underline{V}]\rho$$

$$\frac{\partial p}{\partial t} = - \frac{\underline{B}\times\underline{\nabla}s\cdot\underline{\nabla}P}{B^2} v_\perp$$

$$\frac{\partial \rho}{\partial t} = - \frac{\underline{B}\times\underline{\nabla}s\cdot\underline{\nabla}\rho_M}{B^2} v_\perp$$

where $b_\perp$, $v_\perp$, p and ρ are the perpendicular magnetic field, the perpendicular velocity, the pressure and the mass density perturbations, respectively. The equilibrium magnetic and velocity fields are $\underline{B}$ and $\underline{V}$, respectively, the magnetic field line curvature is $\underline{K}$, the equilibrium pressure, mass density and resistivity are P, ρ_M and η, respectively, and n is the toroidal mode number. It is evident from these equations that normal mode solutions can only be constructed when the toroidal rotation is rigid. The previous work on this subject [3,5] was based on the application of the ballooning representation to the Frieman-Rotenberg energy principle [6]. This energy principle, however, imposes apriori that the solutions obtained be normal modes of the system. Consequently the theory that was developed is limited only to the rigid rotor model. The initial value equations we have derived do not constrain the solutions to evolve as $\exp(i\omega t)$, therefore we are able to investigate the effects of finite velocity shear. The ballooning formalism is still valid when there is shear in the toroidal flow, but the solutions obtained are not normal modes of the system.

Fixed boundary equilibria that model the JET device are obtained with the ATRIME inverse moments code [7]. This code generates axisymmetric MHD equilibria with isothermal toroidal mass flows. The profiles that must be specified are the plasma mass function M(s), the inverse of the safety factor and the plasma flow function $U(s)=0.25M_i\Omega^2(s)/T(s)$, where T(s) is the plasma temperature and M_i is the ionic mass. The plasma pressure can then be constructed from M(s) and U(s) [7]. The equilibria obtained are mapped from the (s,χ,ϕ) magnetic flux coordinates employed in the ATRIME code to the straight field line coordinates (s,θ,ϕ) using the relation $\theta=\chi+\lambda(s,\chi)$, where λ is a periodic renormalisation parameter calculated internally in the code. A numerical JET equilibrium with a thermal beta $\beta_p=4.9\%$, a rotational component of beta $\beta_R=1.1\%$ and Mach number 0.925 at the magnetic axis is generated by specifying $M(s)=0.04(1-4s^3+3s^4)$, $1/q(s)=1-2s^3/3$ and $U(s)=0.023$. As the initial value equations are evolved in time, periodic bursts of ballooning are observed, as is shown in Fig. 1. The mode structures at the peaks of the bursts labelled as a), b) and c) in Fig. 1 are displayed in Fig. 2. The instability structure that develops has strongly ballooning characteristics, but is displaced by 2π in the extended poloidal angle domain from one burst to the next. An instability growth rate that is remarkably linear can be extracted from the peak values of the ballooning bursts. In addition to the profiles required for the equilibrium calculation, the local stability analysis requires the

specification of either T(s) or $\Omega(s)$. Thus it is possible to investigate the effects of plasma rotation and velocity shear with a single equilibrium which we do in this study by varying the temperature profile. A sequence with $\Omega(s=0.85)$ fixed and variable $\Omega'(s)$, where prime indicates a derivative with respect to s, is obtained by choosing $T(s)=1-0.7225s$, $T(s)=1-0.85s^2$, $T(s)=1-s^3$ and $T(s)=1-s^4/0.85$. A sequence with $\Omega'(s=0.85)$ fixed and variable $\Omega(s)$ is obtained with $T(s)=(1-1.026239s^2)^2$, $T(s)=(1-0.804909s^3)^2$ and $T(s)=1-s^3$. At fixed Ω', we find that the growth rate and frequency of the ballooning bursts are insensitive to variations in Ω. On the other hand, for fixed Ω, the frequency varies linearly with Ω' and goes to 0 when Ω' vanishes. The growth rate decreases with increasing Ω' which indicates that the velocity shear has a stabilising effect. This can be understood by noting that two fluid elements on adjacent flux surfaces become physically separated in space as time evolves which inhibits the formation of an instability structure.

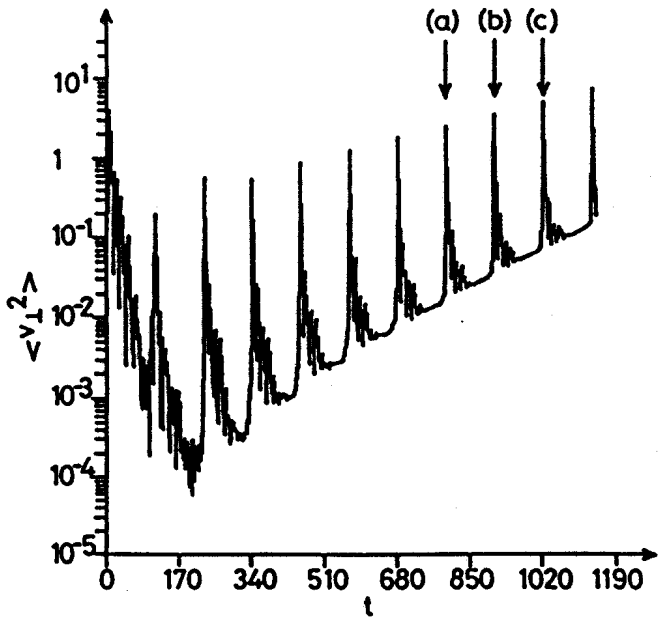

Fig. 1:
The value of $v_\perp^2$ integrated over the extended poloidal angle θ domain as a function of time. The time is normalised to the poloidal Alfvén time.

References

[1] B. Grek et al., Proc. 14th Europ. Conf. on Contr. Fusion and Plasma Phys., Madrid 1987, Europhys. Conf. Abstr. 11D, Part I (1987) 132.
[2] W.G.F. Core et al., Proc. 14th Europ. Conf. on Contr. Fusion and Plasma Phys., Madrid 1987, Europhys. Conf. Abstr. 11D, Part I (1987) 49.
[3] E. Hamieri and P. Laurence, J. Math. Phys. 25 (1984) 396.
[4] R.L. Dewar and A.H. Glasser, Phys. Fluids 26 (1983) 3038.
[5] A. Bhattacharjee, Proc. Workshop on Theory of Fusion Plasmas, Varenna 1987 (edited by A. Bondeson, E. Sindoni and F. Troyon) p.47.
[6] E. Frieman and M. Rotenberg, Rev. Mod. Phys. 32 (1960) 898.
[7] W.A. Cooper and S.P. Hirshman, Plasma Phys. Contr. Fusion 29 (1987) 933.

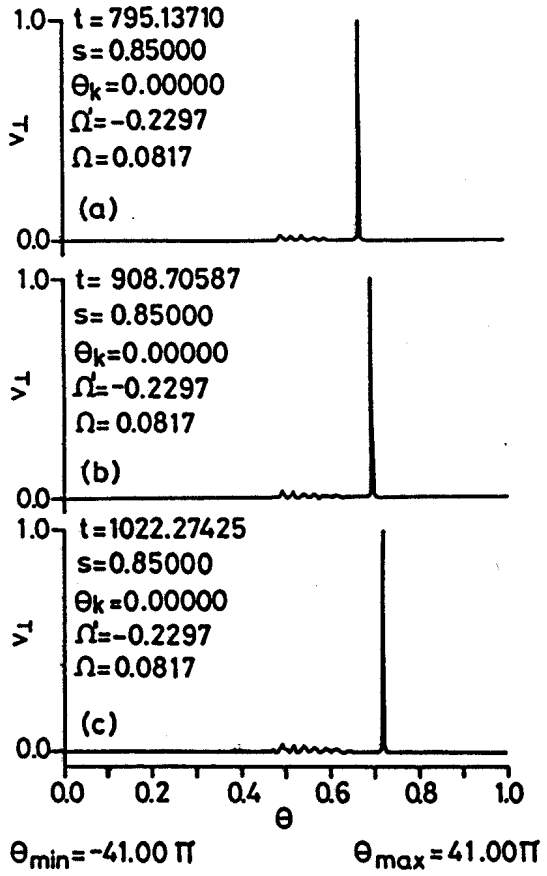

Fig. 2:
The instability mode structures at three different times that correspond to the peaks of ballooning burst labelled with a), b) and c) in Fig. 1, respectively.